TKK Dissertations 145
Espoo 2008

NOVEL DEVICE CONCEPTS FOR OPTICAL WDM COMMUNICATIONS BASED ON SILICON ETALONS, FIBER RESONATORS AND PHOTONIC BANDGAP FIBERS

Doctoral Dissertation

Jesse Tuominen

Helsinki University of Technology
Faculty of Electronics, Communications and Automation
Department of Micro and Nanosciences

TKK Dissertations 145
Espoo 2008

NOVEL DEVICE CONCEPTS FOR OPTICAL WDM COMMUNICATIONS BASED ON SILICON ETALONS, FIBER RESONATORS AND PHOTONIC BANDGAP FIBERS

Doctoral Dissertation

Jesse Tuominen

Dissertation for the degree of Doctor of Science in Technology to be presented with due permission of the Faculty of Electronics, Communications and Automation for public examination and debate in Micronova at Helsinki University of Technology (Espoo, Finland) on the 28th of November, 2008, at 12 noon.

Helsinki University of Technology
Faculty of Electronics, Communications and Automation
Department of Micro and Nanosciences

Teknillinen korkeakoulu
Elektroniikan, tietoliikenteen ja automaation tiedekunta
Mikro- ja nanotekniikan laitos

Distribution:
Helsinki University of Technology
Faculty of Electronics, Communications and Automation
Department of Micro and Nanosciences
P.O. Box 3500 (Tietotie 3)
FI - 02015 TKK
FINLAND
URL: http://nano.tkk.fi/
Tel. +358-9-4511
Fax +358-9-451 3128
E-mail: jesse.tuominen@voyantic.com

ISBN 978-951-22-9650-7
ISBN 978-951-22-9651-4 (PDF)
ISSN 1795-2239
ISSN 1795-4584 (PDF)
URL: http://lib.tkk.fi/Diss/2008/isbn9789512296514/

TKK-DISS-2533

Multiprint Oy
Espoo 2008

ABSTRACT OF DOCTORAL DISSERTATION	HELSINKI UNIVERSITY OF TECHNOLOGY P.O. BOX 1000, FI-02015 TKK http://www.tkk.fi

Author Jesse Tapio Tuominen

Name of the dissertation

Novel device concepts for optical WDM communications based on silicon etalons, fiber resonators and photonic bandgap fibers

Manuscript submitted August 15, 2008	Date of the defence November 28, 2008
☐ Monograph	☒ Article dissertation (summary + original articles)

Faculty	Faculty of Electronics, Communications and Automation
Department	Department of Micro and Nanosciences
Field of research	Fiber Optics
Opponent	Dag R. Hjelme, Professor
Supervisor	Hanne Ludvigsen, Docent
Instructor	Hanne Ludvigsen, Docent

Abstract

Since the invention of the Erbium-doped fiber amplifier in 1987 and the preceding advances in low-loss single-mode fiber technology, fiber optic wavelength-division-multiplexing (WDM) has been the dominant technology of long-haul data transmission in the 1.55-mm region. Modern dense WDM (DWDM) systems can utilize more than 60 transmission channels in the C-band (1530-1570 nm) with a channel spacing of only 25 GHz. The combination of high modulation frequencies and small channel spacing place stringent requirements on the wavelength accuracy and long-term stability of the transmitting lasers.

This Thesis presents simple inexpensive means for referencing and monitoring the channel wavelengths with wavelength references based on solid silicon Fabry-Perot resonators. The precise temperature control of the resonators enables both long-term stability for reproducible locking of lasers and fast sweeps to measure laser wavelengths. By employing unique pilot tones, the wavelengths and power levels of WDM channels can be directly measured from the optical multiplex of the transmission fiber.

In photonic bandgap fibers, a class of photonic crystal fibers, most of the light intensity is guided in the air capillaries of the fiber. This provides the possibility to fill the capillaries with a gas, such as acetylene or methane, having suitable absorption bands coinciding with optical transmission frequencies. The Thesis presents practical applications utilizing these gas-filled fibers as miniature high-resolution absorption cells to provide references for calibrating secondary reference artifacts and measurement instruments. Moreover, multiple absorption lines of acetylene are shown to coincide with standardized DWDM transmission frequencies with adequate accuracy to be used as direct references for the transmission lasers.

The second part of the Thesis deals with the development of novel all-optical and all-fiber components. The gas-filling techniques of photonic bandgap fibers are further exploited to fill a novel lead-glass photonic bandgap fiber with liquid crystal to construct a wideband thermo-optic switch. Also, a passive birefringent resonator made of a length of standard single-mode fiber with reflective end facets is demonstrated to be capable of multi-channel clock recovery in WDM applications where return-to-zero modulation is applied.

Keywords fiber optics, optical resonator, WDM, photonic crystal fiber, clock recovery

ISBN (printed)	978-951-22-9650-7	ISSN (printed)	1795-2239
ISBN (pdf)	978-951-22-9651-4	ISSN (pdf)	1795-4584
Language	English	Number of pages	49p. + app. 37 p.
Publisher	Helsinki University of Technology, Department of Micro and Nanosciences		
Print distribution	Helsinki University of Technology, Department of Micro and Nanosciences		

☒ The dissertation can be read at http://lib.tkk.fi/Diss/2008/isbn9789512296514

VÄITÖSKIRJAN TIIVISTELMÄ	TEKNILLINEN KORKEAKOULU PL 1000, 02015 TKK http://www.tkk.fi

Tekijä Jesse Tapio Tuominen

Väitöskirjan nimi
Uusia laitekonsepteja optiseen aallonpituusmultipleksoituun tietoliikenteeseen perustuen piiresonaattoreihin, kuituresonaattoreihin ja fotonikidekuituihin

Käsikirjoituksen päivämäärä 15.8.2008	Väitöstilaisuuden ajankohta 28.11.2008
☐ Monografia	☒ Yhdistelmäväitöskirja (yhteenveto + erillisartikkelit)

Tiedekunta	Elektroniikan, tietoliikenteen ja automaation tiedekunta
Laitos	Mikro- ja nanotekniikan laitos
Tutkimusala	Kuituoptiikka
Vastaväittäjä	Prof. Dag R. Hjelme
Työn valvoja	Dos. Hanne Ludvigsen
Työn ohjaaja	Dos. Hanne Ludvigsen

Tiivistelmä

Aina Erbiumseostettujen kuituvahvistimien keksimisestä lähtien vuonna 1987 ja sitä edeltävän matalahäviöisten kuitujen valmistusteknologian edistyksestä, aallonpituusmultipleksoidut kuituoptiset järjestelmät ovat olleet vallitseva teknologia pitkissä tietoliikennelinkeissä 1,55 mm aallonpituusalueella. Nykyaikaiset tiheän aallonpituusmultipleksoinnin järjestelmät käsittävät jopa 60 kanavaa C-kaistalla jopa vain 25 GHz kanavavälillä. Suurten modulaationopeuksien ja pienten kanavavälien kombinaatio yhdessä asettavat tiukat vaatimukset aallonpituuksien tarkkuudelle ja lasereiden pitkän ajan vakaudelle.

Tämä väitöskirja esittää yksinkertaisen ja edullisen menetelmän kanavien aallonpituuksien mittaamiseen ja monitorointiin kalibroitavilla mittatyökaluilla jotka perustuvat piistä valmistettuihin Fabry-Perot resonaattoreihin. Näiden resonaattorien tarkka lämpötilasäätö mahdollistaa sekä lasereiden toistettavan lukitsemisen että nopeat taajuuspyyhkäisyt laserien aallonpituuksien mittaamiseksi. Merkitsemällä kanavat omilla alikantoaaltotaajuuksilla, kaikkien kanavien aallonpituudet ja tehotasot saadaan mitattua suoraan siirtokuidun aallonpituusmultipleksoidusta signaalista.

Estokaistakuidut ovat luokka fotonikidekuituja joilla on kapea asetettava päästökaista. Näissä kuiduissa suurin osa valon intensiteetistä kulkee kuidun ilmakäytävissä. Tämä mahdollistaa ilman poistamisen käytävistä ja niiden täyttämisen matalaan paineeseen halutulla kaasulla, kuten asetyleenillä tai metaanilla, joilla on soveltuvia absorptiokaistoja optisten tietoliikennekaistojen kanssa päällekkäin. Tämä väitöskirja esittelee käytännön sovelluksia, joissa kaasulla täytettyjä estokaistakuituja käytetään kompakteina korkean resoluution absorptiokennoina tarjoamaan primäärireferenssejä sekundääristen mittatyökalujen ja mittalaitteiden kalibrointiin. Lisäksi osoitamme useiden asetyleenin absorptioviivojen olevan riittävän lähellä standardoituja lähetyskanavien taajuuksia, jotta niitä voidaan suoraan käyttää lähetyslasereiden taajuuden referenssimittoina.

Väitöskirjan toinen osa käsittelee uusien täysin optisten kuitukomponenttien kehitystä. Estokaistakuitujen kaasuntäyttötekniikkaa on käytetty hyväksi uusien lyijylasikuitujen täyttämiseen nestekiteillä leveäkaistaisen lämpöoptisen kytkimen kehittämiseen. Lisäksi, tavallisesta yksimuotokuidusta valmistetun passiivisen kahtaistaittavan resonaattorin osoitetaan mahdollistavan monikanavaisen kellonpalautuksen sellaisissa järjestelmissä missä ”return-to-zero”-modulaatiota on käytetty.

Asiasanat kuituoptiikka, optinen resonaattori, WDM, fotonikidekuitu, kellonpalautus

ISBN (painettu)	978-951-22-9650-7	ISSN (painettu)	1795-2239
ISBN (pdf)	978-951-22-9651-4	ISSN (pdf)	1795-4584
Kieli	Englanti	Sivumäärä	49 s. + liit. 37 s.
Julkaisija	Mikro- ja nanotekniikan laboratorio, Sähkö- ja tietoliikennetekniikan osasto		

Painetun väitöskirjan jakelu Mikro- ja nanotekniikan laboratorio, Sähkö- ja tietoliikennetekniikan osasto

☒ Luettavissa verkossa osoitteessa http://lib.tkk.fi/Diss/2008/isbn9789512296514

Preface

The work presented in this thesis has been carried out within the Fiber Optics Group at the Micro and Nanosciences Laboratory of Helsinki University of Technology during the years 2001-2008.

I would like to thank several persons who have made it possible to complete the thesis. The supervisor of the work Docent Hanne Ludvigsen I would like to thank for an opportunity to work in the field of fiber optics and her tireless guidance in the scientific world. I am also in gratitude to her for raising the funding for the projects and preparing the grand majority of all applications and status reports.

Dr. Tapio Niemi is thanked for all the guidance I received during my first years in the laboratory. Dr. Tuomo Ritari is thanked for all his efficient work that made our joint papers be published as fast as they were. The personnel of Danish Fundamental Metrology (DFM) are thanked for fruitful cooperation with especially Jan Petersen who is thanked for his expertise and for letting us use his laboratory and equipment in several projects. Numerous people of VTT and Nokia have also generously loaned equipment and shared views of practical optical telecommunications. I especially would like to thank Mikko Söderlund for his valuable input in the channel monitoring trials. I thank Tuomo von Lerber for an interesting project and for the enlightening measurement sessions we had together. Hannu Hoffrén is acknowledged for all his help in carrying out measurements for our joint paper.

Dr. Goëry Genty is acknowledged for his honesty, integrity and advice throughout the years we worked together. Nobody was ever more right than him about ideas being worth trying out or better being left as ideas only. Mikko Lehtonen is thanked for the good company in and outside the office despite regularly beating me in badminton.

I thank all the co-workers who provided invaluable advice and I had the pleasure to work with; Esa Räikkönen, Miika Heiliö, Mikko Merimaa, Markus Hautakorpi, Ossi Kimmelma, Antti Lamminpää, Markku Vainio, Klas Lindfors, and others. I am also very thankful for Risto Myllylä and Alexei Kamshilin for accepting the task of pre-examination and for providing valuable feedback.

The Academy of Finland is acknowledged for funding the projects *Future Electronics Research Programme* and project numbers 124468, 121117 and 120777.

Finally, thank you Ulpu for your love and patience during the work.

Espoo, November 28, 2008

Jesse Tuominen

Table of contents

List of publications

This thesis consists of an overview and the following selection of the author's publications:

[P1] J. Tuominen, T. Niemi, and H. Ludvigsen, "Wavelength reference for optical communications based on a temperature-tunable silicon etalon", Rev. Sci. Instrum. **74**, 3620-3623 (2003).

[P2] J. Tuominen, M. Söderlund, T. Niemi, M. Leppihalme, and H. Ludvigsen, "Device for simultaneous monitoring of the channel wavelengths and power levels in a DWDM system", Journal of Optical Networking **3**, 501-509 (2004).

[P3] J. Tuominen, T. Ritari, J. Petersen, and H. Ludvigsen, "Gas filled photonic bandgap fibers as wavelength references", Opt. Commun. **255**, 272-277 (2005).

[P4] T. Ritari, J. Tuominen, J.C. Petersen, T. Sørensen, T.P. Hansen, H. Simonsen, and H. Ludvigsen, "Gas sensing using air-guiding photonic bandgap fibers", Opt. Express **12**, 4080-4087 (2004).

[P5] J. Tuominen, H. Hoffrén, and H. Ludvigsen, "All-optical switch based on liquid-crystal infiltrated photonic bandgap fiber in transverse configuration", Journal of the European Optical Society – Rapid Publication **2**, 07016 (2007).

[P6] T. von Lerber, J. Tuominen, H. Ludvigsen, S. Honkanen, and F. Küppers, "Multichannel and rate all-optical clock recovery", IEEE Photonics Technol. Lett. **18**, 1395-1397 (2006).

[P7] T. von Lerber, J. Tuominen, H. Ludvigsen, S. Honkanen, and F. Küppers, "Investigation of multiwavelength clock recovery based on heterodyne beats of sideband-filtered signal", Opt. Commun. **271**, 87-90 (2007).

The references to these publications will be denoted by P1-P7.

Author's contribution

The scientific results presented in this work have been carried out during the years 2002-2007. All the publications are the results of teamwork. The author has written the manuscripts of publications [P1-P3], prepared the first version of the manuscript for publication [P5] and contributed to the preparation of publications [P4, P6, P7]. Part of the results has also been presented by him in several international conferences.

For publication [P1], the author designed and constructed the optics, electronics and software for the device with advice from co-author Tapio Niemi. The author also carried out the measurements. For publication [P2] the author participated in building the measurement setup, performing measurements, and analyzing the results with great help and input from co-author Mikko Söderlund. For publications [P3, P4] the author jointly designed the setup, performed the measurements, and analyzed the work with Tuomo Ritari. For publication [P5] the author designed the setup, performed the measurements (with the kind help of Hannu Hoffrén) and performed the analysis. For publications [P6, P7] the author participated in the building and measurement of the initial setup as well as simulating the system that was originally invented by Tuomo von Lerber.

Other peer-reviewed publications to which the author has contributed:

M. Söderlund, J. Tuominen, T. Niemi, H. Ludvigsen, and M. Leppihalme, "Device concept for monitoring DWDM channels", in Proceedings of *29th European Conference on Optical Communication and 14th International Conference on Integrated Optics and Optical Fibre Communication (ECOC-IOOC'03)*, in Rimini, Italy, paper We3.2.2 (2003).

T. Ritari, J. Tuominen, J. C. Petersen, T. P. Hansen, and H. Ludvigsen, "Miniature wavelength references based on gas-filled photonic bandgap fibers", in Proceedings of *30th European Conference on Optical Communication (ECOC '04)*, in Stockholm, Sweden, paper Mo3.3.2 (2004).

T. Ritari, J. Tuominen, J. C. Petersen, and H. Ludvigsen, "Photonic bandgab fibers: Optical properties and device applications", in proceedings of Conference on Information Technology and Communication (ITCom 2004), in Philadelphia, USA, paper 5596-33 (2004).

H. Hoffrén, J. Tuominen, and H. Ludvigsen, "All-optical switching in liquid-crystal filled lead silicate photonic crystal fiber using transverse coupling geometry", in Proceedings of *33rd European Conference on Optical Communication (ECOC 2007)*, in Berlin, Germany, paper We.6.1.6 (2007).

List of abbreviations

CR	Clock recovery
CW	Constant wave
CVD	Chemical vapor deposition
CWDM	Coarse wavelength division multiplexing
DEMUX	Demultiplexer
DFA	Doped fiber amplifier
DFM	Danish Fundamental Metrology
DWDM	Dense wavelength division multiplexing
EDFA	Erbium doped fiber amplifier
F-P	Fabry-Perot
FSR	Free spectral range
LC	Liquid crystal
MMF	Multi-mode fiber
MUX	Multiplexer
NIR	Near infrared
NRZ	Non return to zero
PBF	Photonic bandgap fiber
PCF	Photonic crystal fiber
PRBS	Pseudo-random bit-sequence
RZ	Return to zero
SMF	Standard single-mode fiber
TIR	Total internal reflection
WDM	Wavelength division multiplexing
ZBLAN	ZrFM4-BaF2-LaF3-AlF3-NaF

1 Introduction

The first successful modern optical fibers were drawn in 1956 [1]. The design and fabrication process was improved through the seventies and eighties [2] to create an attractive transmission medium for the telecommunication industry. The fiber offered tens of terahertzs of available transmission bandwidth combined with a loss smaller than 0.2 dB/km. These values were not only completely unheard of using any other type of transmission technology, but also provided such a data carrying capacity that simply was not found of use at the time. However, the global breakthrough of the Internet in the 90s changed the telecommunications bandwidth requirements permanently. Since then, no other transmission medium has been a serious contender for the use of long-haul telecommunications.

The dense wavelength division multiplexing (DWDM) technology is typically used to better exploit the data-carrying bandwidth of optical fibers [3]. The close proximity and high number of transmitting wavelengths calls for inexpensive, yet accurate means to position and monitor the channel wavelengths. The absorption lines of gases have traditionally been used as wavelength references in the optical wavelength range of the electro-magnetic radiation ever since their discovery by Wollaston in 1802 [4]. The spectral locations of the discrete lines are stable and absolute by nature and have only minor dependence on factors like temperature and pressure. This makes them ideal primary references to calibrate the continuously tunable secondary references, such as Fabry-Perot resonators [5], or gratings. Freely selectable wavelengths are needed to reference DWDM transmission channels as molecular absorption lines rarely coincide with the equidistant telecommunications channels.

The development of photonic crystal fibers (PCFs) and devices based on them generated a whole new branch of optics in the late nineties [6]. These fibers have a cross-sectional structure consisting of periodic air holes running along the whole length of the fiber. Thus, the fibers are also referred to as microstructured fibers or holey fibers. Photonic crystal fibers can have a very tight confinement of light in to the fiber core and have therefore mainly found use in optical devices based on nonlinear effects, such as nonlinear switching [7, 8] and supercontinuum generation [9-12]. An interesting special class of PCFs is the photonic bandgap fibers (PBFs). These fibers have an air core that is surrounded by higher index air-silica microstructure that provides guiding of light based on the bandgap effect [13]. Photonic bandgap fibers can guide over 95% of the power in the air regions of the fiber. This makes these fibers interesting for the infiltration of gases in to the capillaries for effective guided interaction over a long length. This provides means to build very simple and compact absorption cells that previously have been realized using cumbersome multiple reflection cells or resonator structures. Oils, dyes and liquid crystals have also been successfully infiltrated in to these fibers to demonstrate numerous novel all-optical device concepts [14-17].

With the huge bandwidth offered by standard telecommunications fibers, the modulation rates of fiber-optic transmission systems keep increasing to levels where the performance of sending and receiving electronics begin to struggle. This makes the all optical, or even all-fiber telecommunication components very attractive. The added benefit of all-optical components is the possibility of parallel processing all the

wavelength division multiplexed channels with one component and in one single fiber. The Erbium-doped fiber amplifier (EDFA) is perhaps the most celebrated such device optically amplifying all channels simultaneously. In a similar fashion, passive all-optical devices have been suggested for the clock recovery (CR) in optical telecommunications receivers [18, 19].

The first part of the thesis describes novel means to reference and measure the wavelength range used in optical telecommunications. First, a Fabry-Perot etalon based measurement artifact is presented [P1]. The etalon used is a solid silicon etalon with high resolution temperature tuning. The device is calibrated to molecular absorption lines of acetylene for consistent accuracy. Two applications are presented for the etalon. The device can function as a tunable wavelength reference for calibrating optical instruments or referencing optical telecommunications channels. Subsequently, the reference was combined with a novel sampling scheme utilizing low frequency pilot tones to measure the wavelengths and power levels of DWDM channels directly from the optical multiplex [P2]. Furthermore, molecular spectroscopy is discussed from the viewpoint of its utilization for WDM channel referencing. The suitable gases are covered with an extra focus on the properties of acetylene. The concept of using gas filled PBFs for building sensitive all-fiber reference artifacts is presented [P3, P4].

The second part of the thesis discusses the development of novel all-fiber components. A realized all-optical switch based on LC-filled PBF is presented making use of a transverse aligning geometry [P5]. Subsequently, new means to extract the clock signal all-optically from the WDM signal are presented [P6, P7]. The method is based on a high finesse fiber resonator with its birefringence tuned to the modulation frequency of the channel bit-rate to generate a beat signal equal to the clock frequency.

2 WDM transmission technology

2.1 Evolution of optical fiber

The principle of guiding light using the phenomenon of total internal reflection (TIR) was first demonstrated in 1840s by Daniel Colladon, a young professor of physics at the University of Geneva. He launched light into a jet of water where it followed the curvilinear path of the water stream [20]. The experiment was spectacular and was reproduced by several people for decades, but eventually only found decorative use.

Later in 1880, hollow tubes with reflective inner surfaces were utilized in an experiment where light was distributed to locations throughout a building from a single intense light source in the basement [21]. The experiment was not completely successful as the mirror surface absorbed too much of the light. The end result was the same as for silica fibers for which attempts were made for a long time to improve the performance by using a reflective silver layer on top of the silica glass. The smaller the fiber diameter was, the higher the attenuation became as the number of reflections per unit length increased.

It was much later after the Second World War when the principle of TIR was again adopted as the most effective means of making optical fiber waveguides. The role of lower index cladding, however, was mostly realized by the use of just air or cumbersome oils or waxes. The first modern type fibers with a doped core and silica cladding were drawn in 1956 by L. E. Curtiss *et al*., who were developing optical fibers for medical imaging purposes, e.g. for gastroscopes, and ureterscopes [1], that relied on a bunch of fibers for image transmission.

In 1965, Kao and Hockham suggested that the attenuation of contemporary silica fibers was caused by remaining unwanted impurities in the fiber material, rather than more fundamental effects like scattering or molecular absorption. They presented optical fiber as a practical medium for telecommunication if the attenuation could be reduced to below 20 dB/km [22]. Extensive research was carried out at the Corning Glass Works soon after that. First they beat the 20 dB/km barrier and then further improved the performance by replacing TiO_2 as the core dopant with Germanium which is used even today. More importantly the physics behind the material absorbtion of the fiber was now understood with the most important effects being Rayleigh scattering and OH-absorption [23, 24].

The achieved attenuation levels of silica fibers rapidly reached the level of ~ 0.2 dB/km at 1.55 μm [2]. This is close to the fundamental minimum level of loss in silica fibers limited by Rayleigh scattering in the near-infrared region. However, even smaller losses of 0.07 dB/km have recently been achieved at wavelengths around 3 μm where the effect of the λ^{-4}–dependant Rayleigh scattering is smaller [25]. The fibers typically used in the mid-infrared region are ZBLAN fluoride fibers.

The evolution and shape of the attenuation curve in optical silica fibers is presented in Fig 2-1. The wavelength region ranging from ~1460 nm to ~1625 nm around the wavelength of minimum attenuation is commmonly referred to as the third transmission window. This transmission band alone has over 20 THz of useable

bandwidth with an attenuation of ~0.2 dB/km and thus shows why fiber-optic telecommunication has been the chosen technology for long-haul transmission links for over two decades.

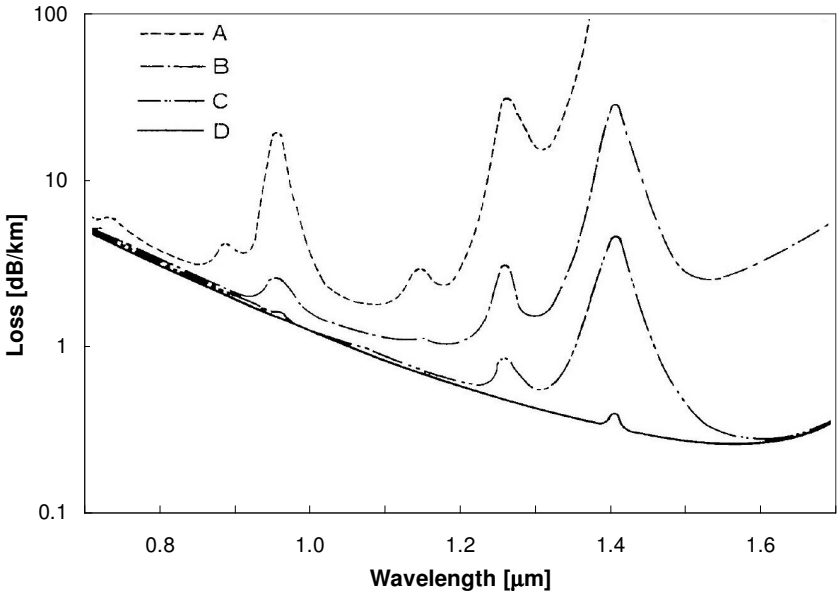

Figure 2-1 **Evolution of the loss spectrum of single-mode fibers during the short period from 1977 to 1980 (A-D) [2]. The drastic reduction of the hydroxyl ion (OH^-) residues in the fiber leave a loss spectrum (D) that is governed by Rayleigh scattering up to 1.55 μm after which infrared absorption becomes the dominant loss mechanism.**

In the mid 90's a new type of fiber emerged, the so-called photonic crystal fibers (PCFs) [6, 26, 27]. These fibers have a cross-section consisting of an array of air holes running uniformly along the fiber length. The PCFs, also referred to as microstructured optical fibers, are all silica fibers with an undoped core. The effectively lower index of refraction outside the core is realised by the holey cladding. The original idea dates back to 1973 when the approach was considered as means to reduce the attenuation in telecommunication fibers by not needing to dope the fiber core [28]. The microstructured optical fibers can have a core much smaller than that of conventional fibers. Consequently, much higher light intensities can be achieved in the core region leading to non-linear effects with more moderate input peak laser powers. The most promising applications for microstructured optical fibers are supercontinuum generation [9-12] and nonlinear pulse switching [7, 8].

Another class of PCFs are the photonic-bandgap fibers [13, 29]. These fibers have an air core which makes the guiding of light using TIR impossible. The confinement is realised by arranging the cladding air holes to create coherent scattering back to the core region. This effect can only happen for a limited wavelength range for a given fiber geometry, usually covering some tens of nanometers. The photonic-bandgap fibers have found use in trace-gas detection [30], molecular spectroscopy [P3, P4], and high power transmission [31].

2.2 DWDM transmission grids

The optical silica-fibers had over 20 THz of useable low-loss data transmission bandwidth already by year 1980. However, the fastest achievable electrical processing and modulation rates are in the gigahertz-range even with the contemporary technology. This drives the use of multiple optical carrier wavelengths to better use the fiber's data transmission capacity. The existence of separate wavelength division multiplexed (WDM) optical channels also enabled the use and development of all-optical add/drop channel-filters.

The concept of WDM dates back to 1970 according to first published reports [32] with fundamental research starting a few years later [33-35]. The early adopted systems were later standardized by the International Telecommunication Union – Telecommunication Standardization Sector (ITU-T) in recommendation G.694.2 [36]. The channels in these coarse-WDM (CWDM) systems were spaced 20 nm apart from each other with the allocated slots typically ranging from 1271 nm to 1611 nm. In modern optical long-haul fiber-links the CWDM systems are superceded by the dense-WDM (DWDM) systems [3] where the channel spacing is more tightly confined around the operation bands of optical fiber-amplifiers. The channel grids in DWDM systems are rooted at 193.1 THz (~1552.52 nm). The spacing between carriers is application dependent and is 200 GHz, 100 GHz, 50 GHz, or 25 GHz. The selected grid spacing controls the number of channel wavelengths that can be supported in a particular transmission band. For instance, using a 50 GHz grid, up to 80 channels can be supported in the C-band (1530 – 1570 nm).

The commonly used binary modulation schemes typically have a spectral efficiency of around 0.4 bit/s/Hz [37]. Thus, the theoretical maximum modulation rate, when using a channel spacing of for instance 100 GHz, would be 40 Gbit/s. When the useable optical bandwidth is fully utilized, a high channel count is used together with a high per-channel data-rate and minimum isolation between channels. This places stringent requirements on the stability and accuracy of the channel wavelengths and motivates the need for 1550 nm region wavelength references [P1, P3] and channel monitors [P2].

2.3 Erbium-doped fiber amplifier

The invention of doped fiber amplifiers (DFA) in 1987 [38, 39] made the utilization of WDM technology even more attractive as now multiple wavelength channels could be amplified simultaneously using all-optical means and making the costly demux-mux and optical-electrical-optical conversions unnecessary at each required amplification stage. The most commonly used type of DFA is the Erbium doped fiber amplifier (EDFA) as it has a relatively broad gain bandwidth right at the absorption minimum of silica fibers around 1550 nm in the C-band [40]. The active medium of an EDFA is Er^{3+} doped single mode fiber through which the WDM signal light passes. Light from a pump laser at 980 nm or 1450 nm is coupled to the same fiber where the pump light is absorbed and the Er^{3+} ions are excited into the $^4I_{13/2}$ state (via

$^4I_{11/2}$ if using a 980-nm pump laser). Once the excitation level is raised above 50% the fiber starts to amplify the WDM channels in the C-band [41]. The gain center location and bandwidth can be tailored to some extend by selecting an appropriate combination of fiber length and excitation level [42]. Doped fiber amplifiers have also been built for the other telecommunication bands introducing alternative dopants such as neodymium [43], ytterbium [44], praseodymium [45] and thulium [46].

3 Tunable etalon based wavelength reference

Fabry-Perot (F-P) interferometer has been a basic building block of optical measurement systems since its invention in 1897 [5] and is the key component in papers P1, P2, P6 and P7. Therefore, the properties of solid F-P interferometers are discussed in detail before presenting the developed applications based on them.

3.1 Properties of solid Fabry-Perot etalons

A Fabry-Perot resonator consists of two reflective surfaces placed at a distance L from each other and the medium in between the surfaces. Typically the medium in optical F-P resonators is air for which the index of refraction is close to unity and thus the dependency on wavelength, temperature or other parameters is negligible. Fabry-Perot etalons are solid optical components with optically transparent material between the reflective surfaces. The reflective surfaces used in solid etalons are typically dielectric quarter wave reflectors. The basic operating principle is, however, the same for all types of F-P resonators.

The transmission, T_r, for a F-P resonator can be written as

$$T_r = \frac{|E_{T_r}|^2}{|E_0|^2} = \frac{\left(1-r^2\right)^2}{|1-r^2\, e^{i2kL}|^2} = \frac{1}{1+\left(\frac{4R}{(1-R)^2}\right)\sin^2\left(\frac{2\pi L}{\lambda}\right)}\,, \tag{3.1}$$

which is referred to as the Airy-function. The wavelengths of transmission maxima, i.e. resonator modes, are found by determining the wavelengths for which $T_r' = 0$ and $T_r'' < 0$. This occurs when the argument of the sine-term becomes zero resulting in a simple and intuitive expression for F-P resonator modes,

$$\lambda_m = \left(\frac{2L}{m}\right) = \left(\frac{2nd}{m}\right), \tag{3.2}$$

in which L can be substituted for nd for solid etalons. Here n denotes the index of refraction and d the thickness. The parameter L in Eq. (3.2) should be treated merely as an effective length. To accurately predict the wavelengths of the resonator modes, the expression should be appended to the form

$$\lambda_m = \left[\frac{2n\left(\lambda, T, I, \sigma\right)\left(d\left(T\right)+2L_{pd}\right)}{m}\right], \tag{3.3}$$

where the following dependences and effects are taken into account with I denoting light intensity, σ material stress and L_{pd} the mirror penetration depth. Applicable examples will be given for the type of silicon etalon used in P1 and P2.

Wavelength and temperature dependency of the index of refraction

Most materials used in optics have a wavelength dependency on their indices of refraction that can alter the index typically by 1-10% in the near infrared region. The index of refraction typically rises at an increasing rate towards shorter wavelengths hinting of a lattice resonance in the ultraviolet region as in Fig. 3-2. The wavelength dependence is often modeled by either using the Cauchy [47] or Sellmeier [48] equations. These equations use coefficients that usually are given for materials instead of refractive index lists. In addition, the refractive index typically has a temperature dependency for which only the first order term is found significant. The combined model used to characterize the refractive index of silicon in P1 and P2 is

$$n_{si} = 3.41696 + \frac{0.138497}{\lambda^2 - 0.028} + \frac{0.013924}{\left(\lambda^2 - 0.028\right)^2} - 2.09 \cdot 10^{-5} \cdot \lambda^2 + 1.48 \cdot 10^{-7} \cdot \lambda^4 + \left(T - T_0\right) \frac{dn}{dT}, \tag{3.4}$$

where T_0 is the normal ambient temperature of 293 K, dn/dT is the temperature coefficient with a value of $1.5 \cdot 10^{-4}$ 1/K and λ denotes the wavelength given in micrometers. The resulting refractive index is plotted for four temperatures in Fig. 3-2.

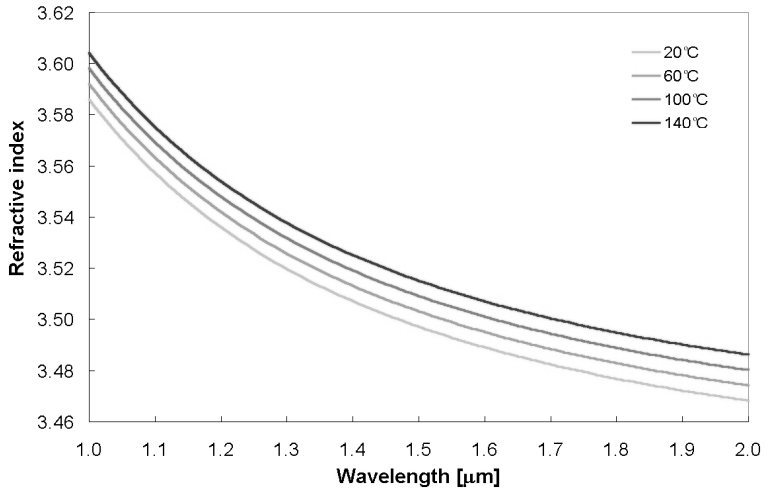

Figure 3-2 Index of refraction of monocrystalline silicon as a function of wavelength and temperature.

Second-order index of refraction of the resonator medium

Kerr-effect is a phenomenon where an electric field in the material modifies the index of refraction of the medium. In this investigation we focus on the case where the electric field is provided by the light itself. This is known as the optical Kerr-effect. Omitting the tensor calculus of the phenomenon, we can simply state that a material has an index of refraction that is intensity dependent

$$n = n_0 + n_2 I \ . \tag{3.5}$$

For most materials, including silicon, n_2 is relatively small making the optical Kerr-effect insignificant for the typical transmission powers and intensities used in optical telecommunications. In the case of resonators though, the intra-resonator intensity can be substantially higher if the mirror reflectivity is close to unity and the resonator finesse is high. In the etalons used in the experiments related to publications P1 and P2, the mirror reflectivities were between 0.6 and 0.8. Thus the optical Kerr-effect can be omitted.

Stress induced variation of the index of refraction

Stress optic effect is a phenomenon where mechanical stress applied to a direction in material induces a change in the index of refraction of material. The magnitude of the effect is dictated by the stress optic coefficient, stress, and the medium thickness. The phenomenon is direction sensitive and can therefore easily create birefringence. The result of this effect is seen in the transmission properties of the silicon etalon used in publications P1 and P2. As the etalon temperature is increased significantly over the ambient temperature, the rectangular shape of the etalon experiences ununiform thermal dissipation, which results in localized thermal expansion based stress. This brings the transmission spectra of the two polarization axes apart from each other. For the silicon etalons in study, we measured wavelength shifts of up to 3 pm for operating temperatures larger than 100 °C. The effect is found to be at its minimum at around 60 °C, which was therefore chosen as the base temperature for tuning. In publication P6, a birefringent fiber resonator was utilized where the birefringence was created and tuned by applying mechanical pressure on the fiber at one direction normal to the fiber. Relative change in the index of refraction achieved was in the order of 50 ppm.

Thermal expansion of the F-P resonator

All material has a tendency to change dimensions, typically expand, when the temperature is changed. In the case of silicon this effect is a few orders of magnitude smaller compared to the change in the refractive index. It is, however, imperative to take it into account to achieve picometer-accuracy.

Penetration depth of dielectric mirrors

The nominal thickness of the etalons used in publications P1 and P2 is 380 μm. However, when quarter-wave dielectric layers are deposited on both surfaces to function as mirrors, the effective length of the resonator is changed. This is due to the fact that light is not reflected at the first boundary of silicon and silicon dioxide but rather at a depth known as the penetration depth. The actual reflection is naturally spread over the various boundaries and the reflected fields interfere producing a reflected wave front that effectively was reflected at the penetration depth. This explains why in Eq. (3.3) a term is added where the penetration depth is added twice to the nominal silicon thickness of the etalon. The penetration depth will be a function of the number of layer pairs used in the dielectric mirrors and will saturate quickly as the number of layers increases. However, this statement only holds when the thickness of the layers actually match the quarter wavelength. To further study the

significance of the effect, a simulation was performed using the etalon material parameters presented in section 3.2. The results are presented in Fig. 3-3.

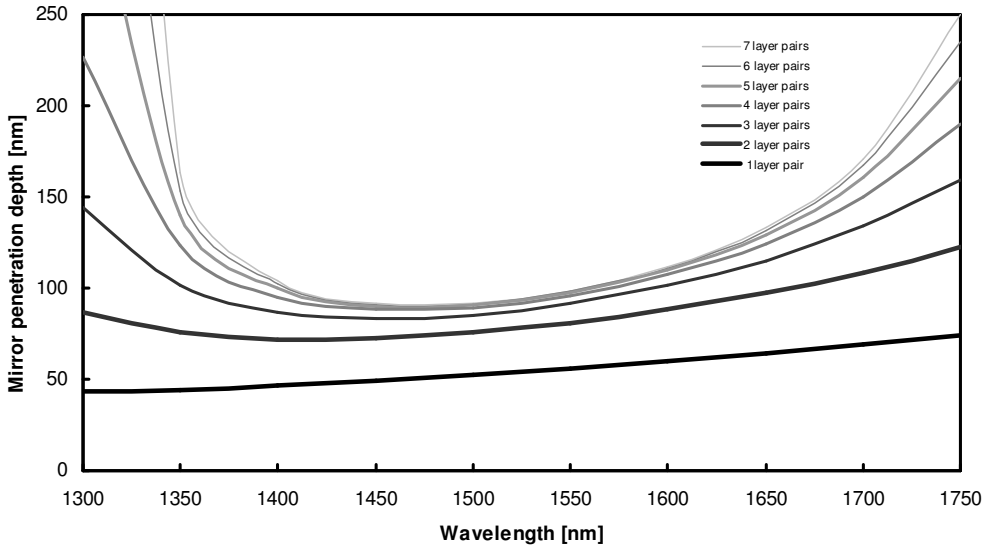

Figure 3-3 Simulation of penetration depth of the dielectric mirrors of an etalon as a function of wavelength and the number of layer pairs.

It should be noted from the simulation, that the number of layer pairs used to generate the mirrors is crucial in the predictability of the fringe wavelengths over a larger wavelength region. If the etalon reference should work at both the 1.3 μm and 1.5-1.6 μm bands of optical telecommunication, then a maximum of three layer pairs should be used for the etalon mirrors. In the case of low refractive index contrast between the low-index and high-index dielectric layers, the penetration depth will become significantly larger than in the case of for example fiber Bragg gratings.

3.2 Tunable silicon etalon as a wavelength reference

Silicon offers a number of attractive features for which it was chosen as the material of the etalon used in the work described in papers P1 and P2 [49, 50]. The fabrication techniques and optical properties of silicon are very well known due to the advances in semiconductor technology and research in opto-electronics. The matured fabrication technology of silicon guarantees precision and repeatability in fabrication and most interestingly silicon can be considered optically transparent for wavelengths longer than 1.1 μm deep into the far infrared range [51].

The developed etalon chip was fabricated of a double-side polished silicon wafer with a nominal thickness of 380 μm. This is a standard thickness for a 3-inch silicon wafer. Dielectric quarter-wavelength mirrors were deposited on both sides of the wafer to create a high finesse resonator. Three pairs of SiO_2 and Si_3N_4 layers were deposited on both sides using chemical vapor deposition (CVD) processes. The indices of refraction for these layer materials are 1.45 and 2.00, respectively, in the 1.55-μm region [52]. The final layer structure of the etalon is presented in Fig. 3-4.

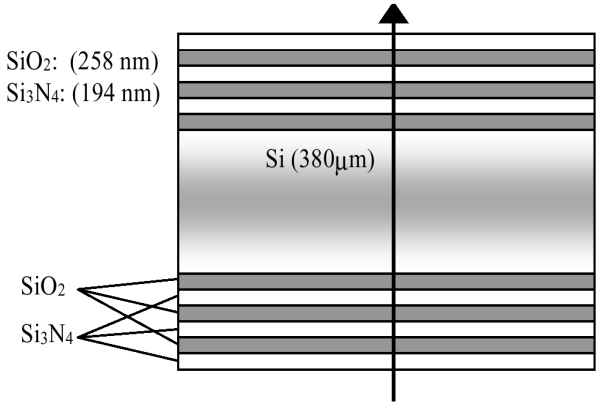

Figure 3-4 **Layer structure of the silicon etalon. Three layer pairs of silicon dioxide and silicon nitride are used on both sides of the silicon substrate as quarter wave mirrors. The direction of light is indicated by with an arrow.**

Two resistors are deposited on the surface of the etalon for heating and temperature sensing. Using accurate digital control combined with fast analog feedback loop, the temperature of the etalon can be tuned in 300 μK steps corresponding to around 200 fm steps in the transmission spectrum of the etalon fringes in the 1550 nm range. Three evolutions of the solid etalon were designed. The first version relied on the silicon-air boundary alone to act as a resonator mirror [49], the second version was designed with the quarter-wave mirrors as presented [50, 53, 54] and the third version was an attempt to further miniaturize and improve the design parameters. These two latter versions are presented in Fig. 3-5.

A) **B)**

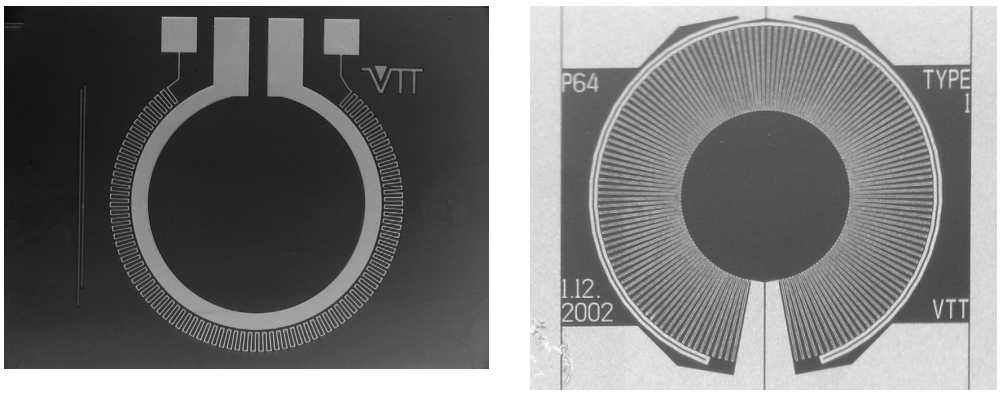

Figure 3-5 **a) The second evolutionary version of the temperature tunable solid silicon etalon as used in publications P1 and P2.**

b) The third generation etalon has improved mirrors that are better matched to a quarter of a wavelength at 1.55 μm. The diameter of the center spot was reduced to 1 mm from the previous ~4 mm.

Careful attention was placed on the design of the control electronics controlling the etalon temperature. The result was an enclosed device that connects to a parallel interface of a computer. Subsequently, control software was written with the sole purpose of taking a target wavelength as an input parameter and calculate and set a needed etalon temperature to position one of the transmission fringes accurately on the wavelength. This secondary reference artifact was calibrated to a transmission line of $^{13}C_2H_2$ and, subsequently, measured against other transmission lines of acetylene using beat frequency detection to measure the error. The largest absolute wavelength errors recorded were on the order of ~1 pm.

3.3 Active WDM channel monitoring

The fast and precise tunability of the developed silicon etalon make its adaptation for wavelength monitoring an attractive possibility. With a sub-picometer scanning resolution and a wavelength sweeping-rate of 0.2-2 nm/s, the device is readily capable of performing wavelength measurement of laser lines with high accuracy. The operating principle would be the measurement of transmitted signal while the etalon fringe is swept over the laser line. Since the FSR of the etalon is relatively small, an approximate initial guess of the wavelength to be measured should be made with accuracy better than FSR/2 in order to know which of the etalon fringes is actually performing the sweep of the laser line. Assuming that the etalon bandwidth is considerably broader than the laser line, modulated or CW, a single sweep should produce a waveform identical to the fringe shape of the etalon. Even if the modulated laser line would be broad in comparison to the fringe, the resulting signal would at least be symmetrical around the peak wavelength, which alone would be sufficient for the accurate determination of the laser center wavelength. The signal of a performed sweep over a laser line is presented in Fig. 3-6. A detection threshold level is set to 5 dB below the peak value and a second order polynomial fit is performed for the points above the level. From the resulting parable the peak power and wavelength can be easily deducted. Directly measuring single lines, the absolute wavelength accuracy of the etalon reference artifact [P1] is directly applicable with no measurable added uncertainty or error. A relative wavelength accuracy of as small as ~10 fm was measured. The presented scheme will potentially not be directly applicable for modulation and transmission techniques such as carrier suppressed and single side-band transmission systems as they do not have a clear carrier wavelength with symmetrical sidebands.

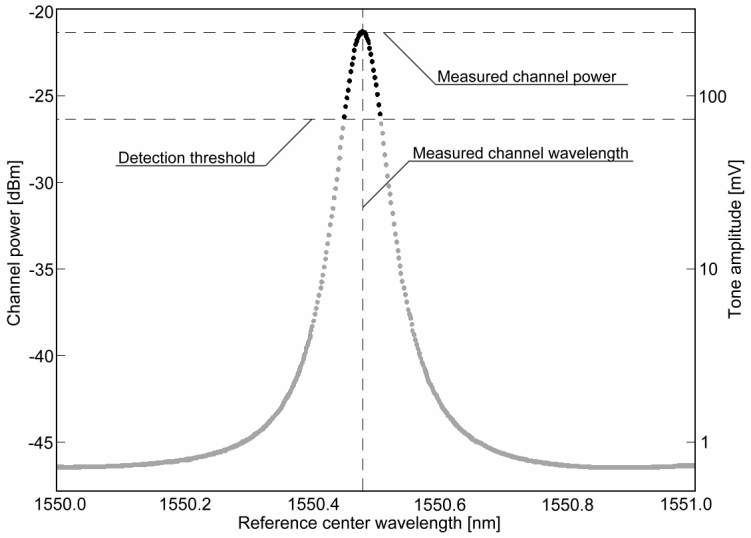

Figure 3-6 **Resulting signal of the tunable silicon etalon scanning over a laser line in small increments. By performing a quadratic fit to the peak area, the center wavelength can be deducted with a resolution of ~10 fm.**

The direct measurement of the transmitted light, as previously presented, will only work when a single laser line is to be measured. In the presence of several lines, they will most probably coincide with multiple fringes of the etalon at some point of the scan and result in superimposed results that can not be distinguished from each other. To overcome this, the utilization of weak individual pilot tones was suggested and successfully demonstrated [P2]. The proposed scheme involves a novel filtering algorithm that facilitates the computation at each discrete etalon scanning point. For each WDM channel to be scanned, and for each scanning point, the data carrying gigahertz-range frequencies are filtered out at the receiver and only the multiplex of the kHz-range pilot tones is preserved. Subsequently, this signal is converted from analog to digital, utilizing a sampling frequency exactly four times greater than the tone to be measured. The principle of this sampling scheme is illustrated in Fig. 3-7.

The sampling is conducted in such a way that every fourth sample is always summed together, i.e., the 1st, 5th, 9th, etc. samples are added to Σa, the 2nd, 6th, 10th, etc. to Σb, and so on. This results in four sums Σa, Σb, Σc, and Σd of which the peak-to-peak tone amplitude can be calculated as

$$V_{pp} = \frac{4}{n}\sqrt{\left(\Sigma_a - \Sigma_c\right)^2 + \left(\Sigma_b - \Sigma_d\right)^2}, \qquad 3.6$$

where n is the total number of samples. The number of sampled periods should be chosen to be at least hundreds of tone periods, but small enough so that transmitter and receiver clocks for the pilot tone generation and sampling should not differ by more than ~π/4 in phase over the entire time of the sampling. Because calculating a sum is perhaps the easiest mathematical function that a processor can perform, this form of digital filtering will put minimal hardware requirements for the receiver hardware [55, 56].

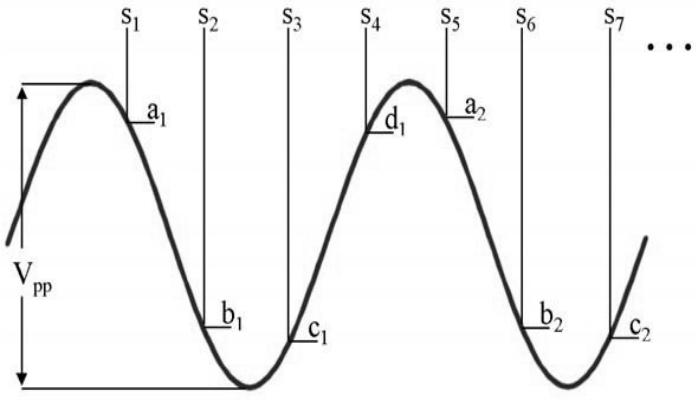

Figure 3-7 Principle of the tone frequency sampling system utilized in the WDM monitoring scheme presented in P2.

The proposed wavelength and power-level monitoring scheme was trial tested jointly with VTT in a four-channel WDM testbed. Absolute accuracies of better than 5 pm and 0.1 dB were reported for the channel wavelength and power level [56]. The performance of the proposed system with a higher number of channels was studied through simulation and the results are presented in P2.

4 Gas-filled photonic-bandgap fibers as wavelength references

Absorption lines of various atomic and molecular species have been used for wavelength references already for nearly two centuries because of their stable and absolute nature [4]. Gases such as acetylene, methane, and carbon dioxide exhibiting rotational-vibrational absorption lines in the near-infrared region have been used for referencing and calibrating fiber-optic measurement equipment from the beginning of fiber-optic telecommunication technology. In our work, acetylene was widely used as a benchmark for wavelength accuracy [P1], for gas sensing experiments using PBF [P4] and for realization of sealed PBF-based wavelength references for WDM technology [P3]. In the following, the properties of acetylene and the benefits of using it in conjunction with fiber-based references are discussed.

4.1 Gas spectroscopy of acetylene

The energies of vibrational modes of a wide range of molecules, expressed as photon frequency, lie in the mid infrared region of spectrum. This results in the near infrared (NIR) absorption typically to originate from vibrational overtone or combination modes. Furthermore, when a vibrational overtone or combination mode is associated through selection rules with the allowed rotational modes, an absorption band is created. Due to the many possible combinations of vibrational rotational energies, the absorption bands easily become numerous and very complicated. They typically consist of hundreds of absorption lines solely in the NIR region of the absorption spectrum. To keep the complexity to a minimum, symmetrical molecules with only few atoms are generally preferred. A few interesting molecules for referencing the wavelength range used by optical WDM technology in the NIR are presented in Fig. 4-1. One of the most attractive molecules to use is acetylene (C_2H_2).

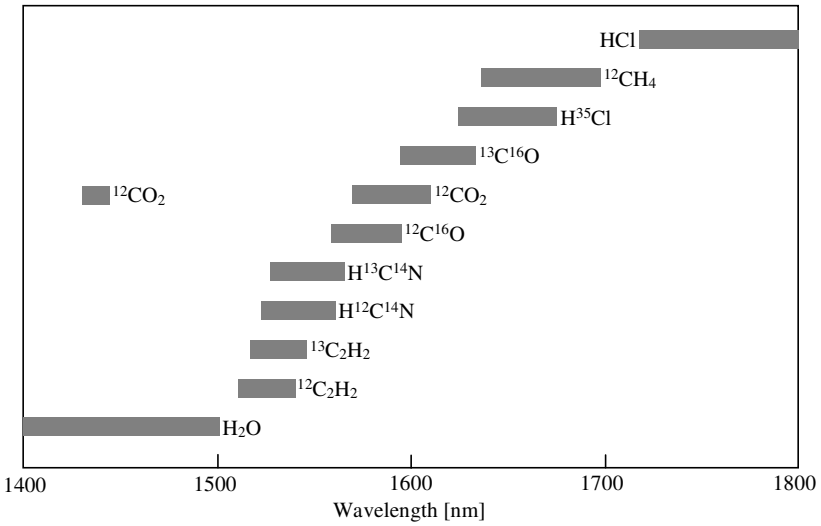

Figure 4-1 Commonly used gas species having absorption bands in the usable WDM transmission range.

Acetylene is a linear four-atomic molecule with thus 3N-5 = 7 normal modes of vibration. These vibrational modes and their notation are presented in Table 4-1. Modes ν_1, ν_2 and ν_3 are stretching vibrations along the molecule axis, whereas ν_4 and ν_5 are bending modes with two possible planes of vibration caused by the two-fold symmetry of the acetylene molecule. The most widely used WDM reference band is the $\nu_1 + \nu_3$ combination band for both $^{12}C_2H_2$ and $^{13}C_2H_2$. The structure of this absorption band is presented in Fig. 4-2.

Table 4-1 **Vibrational modes of acetylene. Seven degrees of freedom can be distinguished for a linear molecule with four atoms. Note that the modes ν_4 and ν_5 have two possible planes of vibration. The energy levels are only approximate as they differ slightly from band to band. The energy is given in 1/cm to facilitate the calculation of the wavenumber corresponding to an absorption band.**

Vibration mode	Denotation	Energy [1/cm]	Description
	ν_1	~3370	Symmetrical CH stretch
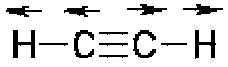	ν_2	~1970	CC stretch
	ν_3	~3280	Asymmetrical CH stretch
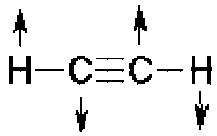	ν_4	~610	Symmetrical CH bend
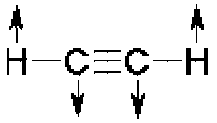	ν_5	~760	Asymmetrical CH bend

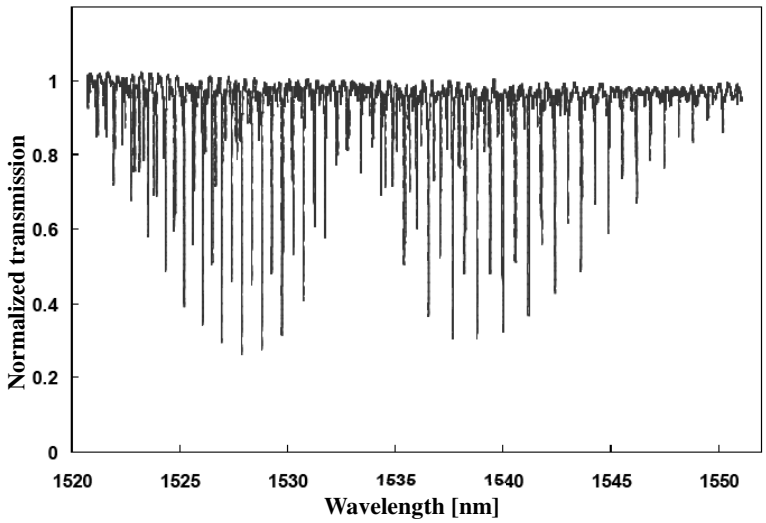

Figure 4-2 **Absorption lines of $^{13}C_2H_2$ measured for a conventional 14 cm long gas cell. Fluctuations in the background level are caused by accidental etalons.**

The acetylene molecule consists of two carbon and two hydrogen atoms, both of these having multiple stable isotopes. Carbon has two stable isotopes, ^{12}C and ^{13}C, their natural abundances being 98.93% and 1.07%, respectively [57]. Since each acetylene molecule has two carbon atoms, three variations of acetylene can be distinguished as far as carbon isotopes are concerned, $^{12}C_2H_2$, $^{12}C^{13}CH_2$ and $^{13}C_2H_2$ with natural abundances of 97.87%, 2.18% and 0.011%, respectively. Despite the low natural probability of existence, $^{13}C_2H_2$ can be isolated and it is widely used as a primary wavelength reference because its absorption band is closer to 1.55 µm than the one of its lighter $^{12}C_2H_2$ version [58]. Hydrogen also has two stable isotopes ^{1}H and ^{2}H, where the latter is more widely known as deuterium and often denoted by D. However, the abundance of deuterium on Earth is only 0.015% making the presence of C_2HD and C_2D_2 acetylene rare in nature. However, their absorption spectra are well examined and documented [59-62]. Especially C_2HD is commonly used as a wavelength reference in the 1064 nm region.

Similar to all other gas absorption lines, acetylene lines suffer from pressure-induced self-broadening. Consequently, pressures below ~100 mbar are preferred to keep the measurement resolution at a high level to assure that weaker lines will not disappear in to close lying stronger lines. The absorption lines have an approximate line dependent pressure broadening of up to 10 MHz/mbar [63]. However, pressure shifts put a more stringent requirement on the maximum allowed pressure level if high accuracy is required. In the $\nu_1 + \nu_3$ bands of acetylene, pressure shift offsets up to 0.6 MHz/mbar and 0.3 MHz/mbar have been reported for the R- and P-branches, respectively [63, 64].

4.2 Realized photonic bandgap fiber references

Photonic bandgap fibers guide light by the bandgap effect, rather than by the conventional total internal reflection mechanism. The core is typically made by removing 7 or 19 of the capillaries from the center of the fiber leaving the core to be of nothing more than air. This in turn makes a large part of the light intensity in the fiber propagate in air rather than in silica. Up to 98% of the power has been reported to be carried in the air regions of a PBF [65, 66]. Microscope images of the utilized PBFs are presented in Fig. 4-3.

A) B)

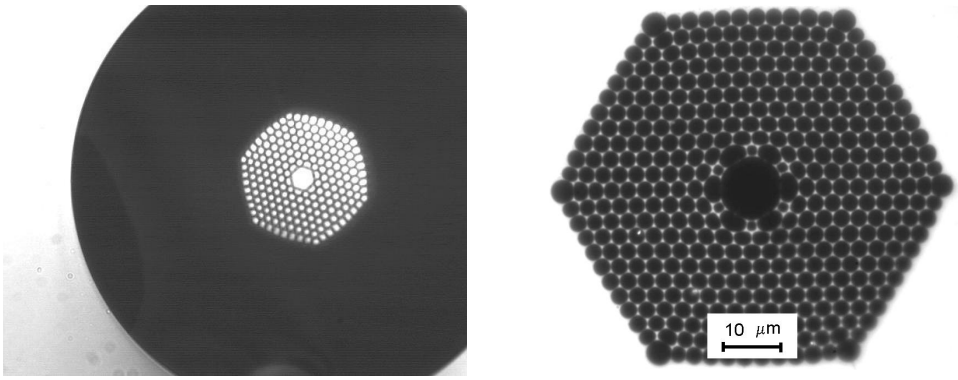

Figure 4-3 **a) A photograph of the cross section of the PBF used in P4. The cladding is fabricated from hollow capillaries and the core by removing seven of the capillaries. 1510-1570 nm**

b) A photograph of the central part of the cross section of the PBF used in P3. This is an earlier version of AIR-10-1550 by *Crystal Fibre A/S* having a broader transmission bandwidth from 1400 to 1600 nm.

A setup for evacuating, filling and sealing the PBF was built around a brass cylinder as shown in Fig. 4-4b. The PBF was readily spliced to a SMF that was either coiled inside the chamber or taken out from the middle of the end facet for live measurement. The open end of the PBF was butt coupled to a multimode fiber on a v-groove in the center of the chamber. A vacuum line was connected to the side of the chamber for the evacuation of air from inside the chamber and the fiber capillaries. A second vacuum line was connected to the other side of the chamber for filling the chamber to a desired pressure. A pressure gauge was connected to this vacuum line for registering and monitoring the chamber pressure. After filling the chamber with gas, a few minutes was waited for the gas concentration to equalize through the length of the capillaries. The absorption characteristics of a single line were usually monitored while filling to see when full absorption strength was achieved.

After a successful filling and a preliminary measurement, the filled fiber is sealed. The chamber has an applicator needle for adhesive mounted directly on top of the butt coupling with a valve right outside the chamber. A drop of UV-curable index-matching adhesive was dropped between the fiber ends and cured using a solid UV guiding rod and an external UV-source. The sealing setup is presented in Fig. 4-4a. At room temperature the UV-adhesive has a boiling pressure of ~10 mbar when lit by the UV. For sub 10 mbar filling, this forced us to first apply the drop, then rapidly raise the pressure above 10 mbar and only then activate the UV. This pressure increase resulted in that the adhesive was pushed a short distance in to the capillaries slightly increasing the loss of the final coupling. The attenuation typically increased by 2-4 dB in the application and curing stages of the adhesive.

A) **B)**

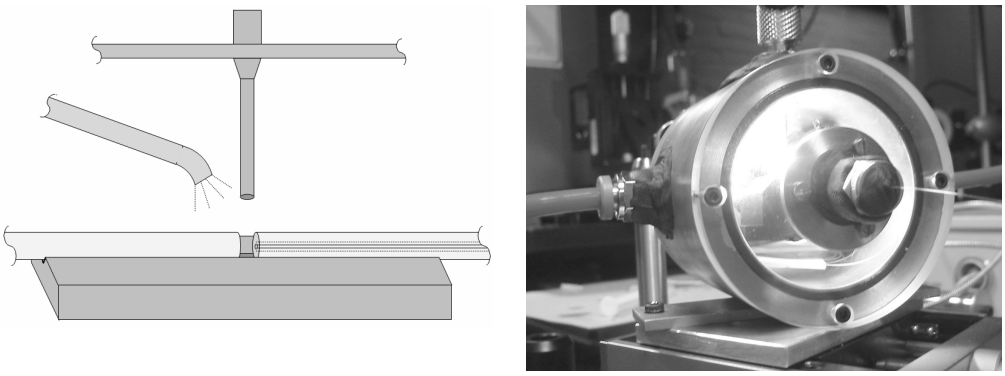

Figure 4-4 **a) A schematic picture of the gas filling setup. The PBF is placed on the right and is aligned with the conventional fiber on the left. A small gap is left between the fiber facets for the gas flow. On top is the sealant application needle. A UV-guide is at the left to cure the sealant.**

b) The chamber (built by DFM in Denmark) in to which the filling and sealing setup was assembled.

The performance of a filled PBF-cell was compared with a traditional absorption cell. The length was 1 m for both reference artifacts and the pressure was chosen to be set to 10 mbar. The gas was standard grade acetylene with 98% $^{12}C_2H_2$. The effective free space length of the fiber-cell was calculated from the results to be 78±5 cm. This is slightly less than the fraction of light propagating in the air and is most probably caused by imperfect evacuation of the air or error in final filling pressure. The results are presented in Fig. 4-5. In the trace of the PBF reference the background line has large fluctuations the source of which remains uncertain. These fluctuations were typical for the early type AIR-10-1550 and the problem was greatly diminished in the later type.

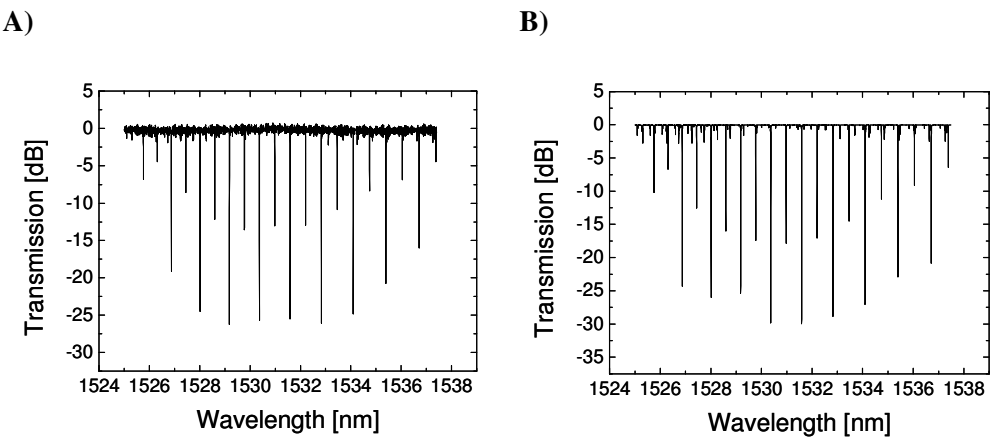

Figure 4-5 The absorption spectra of the P-branch of acetylene near 1530 nm at 10 mbar: a) in a 1 m long PBF (AIR 10-1550 from *Crystal Fibre A/S*) b) in a 1 m long absorption cell measured at DFM in Denmark

Usually, moderately low pressures of less than ~50 mbar are desired to avoid the excess pressure broadening and pressure shift of the absorption lines which are unwanted for reference artifacts. Thus for weakly absorbing bands, it is desirable to increase the interaction length between light and gas to obtain a sufficient signal level. In case of a fiber-based reference, the length is not an issue as the light is guided and practically any desired length can be coiled into a matchbox size enclosure. This benefit gives much more freedom in first choosing the desired pressure for resolution and secondly the optimum fiber length for desired absorption strength for the given application.

5 All-optical switching using liquid crystal filled photonic crystal fibers

5.1 Properties of liquid crystals

First scientific reports of the existence of liquid crystals (LC), a material halfway solid and liquid, date back to the late 19th century when cholesterol and related organic substances were studied [67, 68]. It was noticed that when cholesteryl benzoate is heated, it first melts to an opaque liquid at 145 °C and later becomes a clear liquid at 178 °C clearly indicating that changes in the material are possible within the liquid phase. The different LC phases between the solid phase and isotropic liquid phase are referred to as mesophases, which are thermodynamic phases with physical properties between those of pure liquids and pure solids. The liquid crystals were considered as merely a curiosity for nearly a century before the first practical liquid crystal displays were built in 1967 [69].

Liquid crystals are a class of fluids that have a number of different mesophases with varying levels of molecular order. With increasing temperature, the LC can go through several ordered mesophases until it reaches the isotropic mesophase where all positional and orientational order is lost as illustrated in Fig. 5-1. Single LC-molecules typically are highly birefringent making the index of refraction of the entire substance anisotropic for mesophases that have a degree of orientational order, e.g. the nematic mesophase. Most applications are based on LCs that have their nematic mesophase at room temperature [70]. The orientation of the nematic LC molecules is affected not only by the confining space and surface preparation, but can also be controlled by using external influence such as electric and magnetic fields.

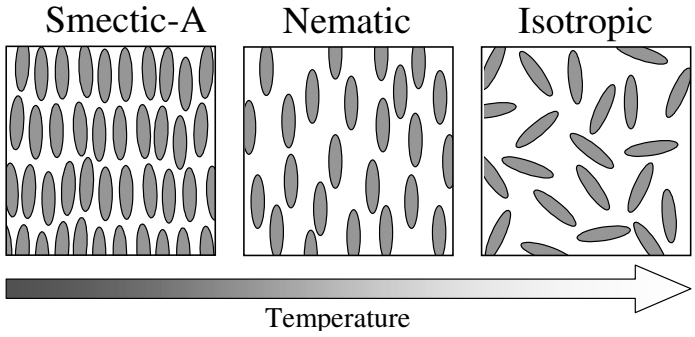

Figure 5-1 Liquid crystal order and orientation in the smectic-A, nematic and isotropic liquid crystal mesophases.

5.2 Liquid crystal based fiber-optic switch

Since the invention of photonic-crystal fibers, researchers have toyed with the idea of infiltrating the air capillaries with optically active materials such as gases [71], index-matching oils, or fluorescent dyes [72]. Various devices have been proposed making use of LC infiltrated PCFs, with optical switches being one interesting group of such devices.

Optical switching based on a liquid-filled PCF was first demonstrated by Eggleton *et al.* [73]. The device consists of a silica-core PCF with a tapered section and moveable oil plugs in the cladding holes. When the oil plugs where positioned in the tapered section, the fiber loses its guiding properties. Later LC was infiltrated in a PBF whereby modifying it into an index-guiding fiber. The transmission of the generated fiber was controlled by an external electric field. At the operating wavelength of 633 nm, the transmission was attenuated by 30 dB with a 60 V alternating control voltage [16]. This kind of device was presented in 2003 [17, 74]. Switching action was based on temperature tuning utilizing the smectic-A to nematic mesophase transition. An extinction ratio of 60 dB was achieved as the nematic mesophase was scattering for all wavelengths measured.

By doping the nematic LC with a dye Alkeskjold *et al*. realized an optically tunable device [14]. The ~3 mW control pulses were absorbed by the dye modifying the index of refraction of the LC resulting in a shift of the transmission bandgap. By positioning a signal laser at the bandgap edge, up to 2 kHz modulation was achieved.

In 2004 Nguyen *et al.* demonstrated that the microstructure of PCFs can be used as thermally controlled optical switch where light is transmitted along the radial direction through the fiber cross-section [15, 75, 76]. The operation was based on moving fluid plugs in the capillaries to the position of the transverse light transmission.

In our work, we explored the possibility of combining LC-filled PCF, optical switch actuation, and transverse fiber geometry [P5]. Light was coupled from a standard single-mode fiber to the side and through of a LC-filled PCF and back to a standard fiber again as illustrated in Fig. 5-2.

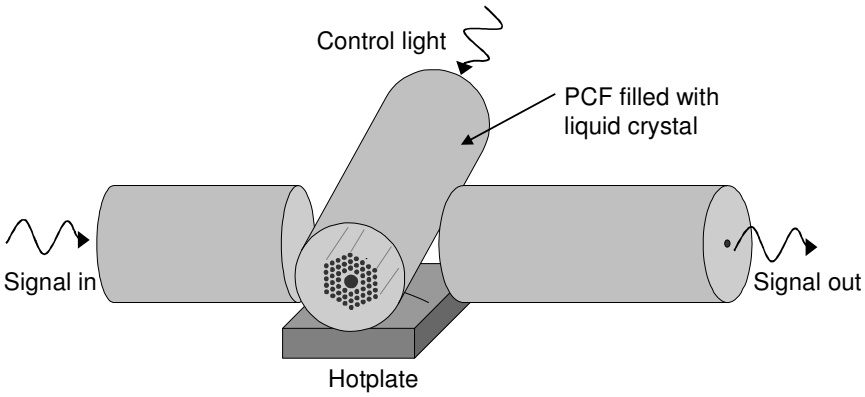

Figure 5-2 Geometry of the explored LC-filled PCF based switch design. Signal light is transmitted transversally through the PCF while light guided along the PCF is used to actuate the switch through nematic to isotropic mesophase transition.

The distances of the fibers were tuned for the PCF to act as a lens to couple as much of the signal light back again in to the fiber. The temperature of the LC-filled fiber was tuned just below the nematic to isotropic mesophase transition temperature. To actuate the switch, 1550 nm light pulses are guided along the LC-filled PCF and are partly absorbed by the LC and its temperature is raised taking the LC to its isotropic mesophase. In the isotropic state, the refractive index of the LC approximately matches the one of the lead silicate fiber material minimizing the transverse transmission losses. In the nematic state, both the LC itself and the LC-filled fiber microstructure become highly scattering giving an extinction ratio from 9 to 26 dB. The advantage of the explored switch design is the possibility to use ~1550 nm control light wavelength to actuate ~1550 nm signals with extreme isolation [77]. The required actuation power levels of 10 mW could greatly be reduced by using a dye-doped LC.

6 All-optical multi-channel clock recovery

The use of a clock signal is a fundamental feature of virtually all telecommunication, especially digital. Many older electric data transmission standards rely on a separate channel for the clock signal that dictates when the data signal should be sampled and read. In a similar way, sacrificing one channel wavelength for a clock signal in optical WDM systems would be limited to relatively short distances, as dispersion would shift the clock and data channels in time relative to each other. Therefore the clock signal is extracted from the data bit-stream itself in optical telecommunication systems. This function is commonly referred to as clock recovery.

In optical communication systems of today, the clock recovery process is performed in the electric domain after the optical signal is detected and amplified. A more modern alternative for the electric clock recovery is all-optical clock recovery. All-optical means for clock recovery have three interesting benefits over the electric domain process. Firstly, electric CR directly results in the fact that the clock recovery must be performed individually for each WDM channel. Optical CR, however, possesses the possibility to recover the clock signal for each channel directly from the WDM stream using one single optical component. Secondly, this optical component can be a passive device resulting in a simplified and potentially more efficient system. Thirdly, electric processing for data-rates exceeding 40 Gb/s is proving cumbersome. Instead, CR with passive optical components can become easier to perform the larger the data-rate is. In papers P6 and P7, we show two examples of all-optical CR using a F-P resonator in which the three potential benefits are realized.

6.1 All-optical clock recovery with Fabry-Perot resonators

Using F-P resonators for optical CR is not a completely new innovation in its simplest form where the bit-rate and resonator FSR are made to match [19]. This results in the carrier frequency and the modulation sidebands to match resonator fringes. When the photon lifetime of the resonator is significantly greater than the length of one single bit, these frequencies can be regarded as CW lines once they pass the resonator. Furthermore, having two or more CW lines at equidistant spacing will result in a low frequency beat signal at a frequency identical to the frequency difference of these lines.

The tuning of a F-P resonator, as described above, can be tricky because two critical requirements must be satisfied simultaneously. First, the position of one fringe must match the carrier frequency of the WDM channel. Secondly, the FSR needs to accurately match the bit-rate. The tuning is difficult, due to the fact that only one parameter, the effective length, can be adjusted in the F-P resonator to match two requirements. Therefore in practice, the WDM channel frequency must be fine-tuned to suit the clock recovery resonator. This may be satisfactory at research level, but such backwards tuning will not be accepted by the telecom market or standardizing bodies. The situation becomes more complicated for the clock recovery of multiple channels. For a standard F-P resonator CR setup to handle multiple channels, a third requirement must be satisfied by the resonator effective length. This requires that the channel spacing is an integer multiple of the resonator FSR. The chances of

succeeding in tuning such a system even in a laboratory to continuously operate for more than a few microseconds are slim.

To illustrate the nature of resonator based clock recovery, the signals for the data and clock recovery is presented in Fig. 5-1. Each 1-bit is a pulse of light that brings new energy to the resonator and thus strengthens the clock signal. For each 0-bit, energy is only leaked out at a rate depending of the photon lifetime of the resonator making the pulses weaker after successive zeros. The clock signal decay at the end of the data packet and the first clock pulse will appear when the first 1-bit is received. Therefore, no clock will be generated for any possible leading zeros in the packet. To overcome this, many transmission systems either use a preamble at the beginning of a packet or the channel is coded so that no digital silence is allowed. In a similar way, the ratio of ´1´ and ´0´ bits is usually coded to be close to unity.

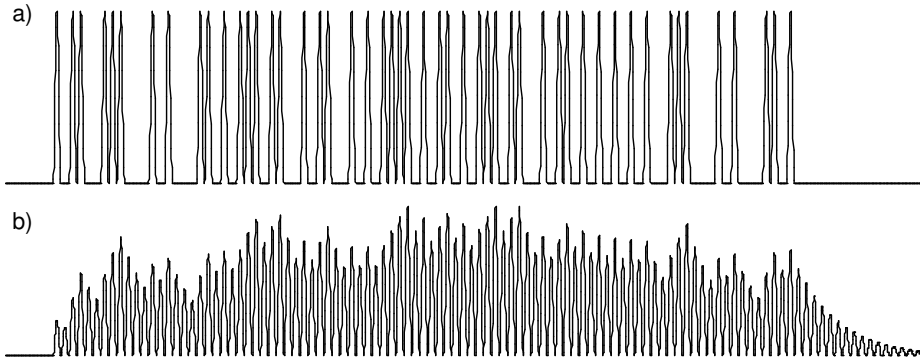

Figure 5-1 A simulated example of a) 100-bit packet of RZ-coded data and, b) its clock recovery signal.

It is imperative that the data-stream is return to zero (RZ) coded like the random bit sequence presented in Fig. 5-1. The spectrum of RZ-coded random data has strong sidebands separated by the bit-rate from the carrier frequency. These narrow sidebands do not appear in the non return to zero (NRZ) coded signal spectrum and NRZ can therefore not be used for F-P resonator based CR. These sidebands, together with the carrier frequency, are the spectral lines that are filtered by the F-P resonator and beating together to create the clock signal. The difference in spectra between RZ and NRZ coded signals is presented in Fig. 5-2. The simulations in Fig. 5-2 were conducted using square-pulsed data and therefore show multiple harmonics. This represents a case of no frequency mask and is for illustrative purposes only. In practice, the spectra of binary telecommunication signals are tried to be kept as narrow as possible without losing information. This also enables narrow channel spacing for all systems, including DWDM systems.

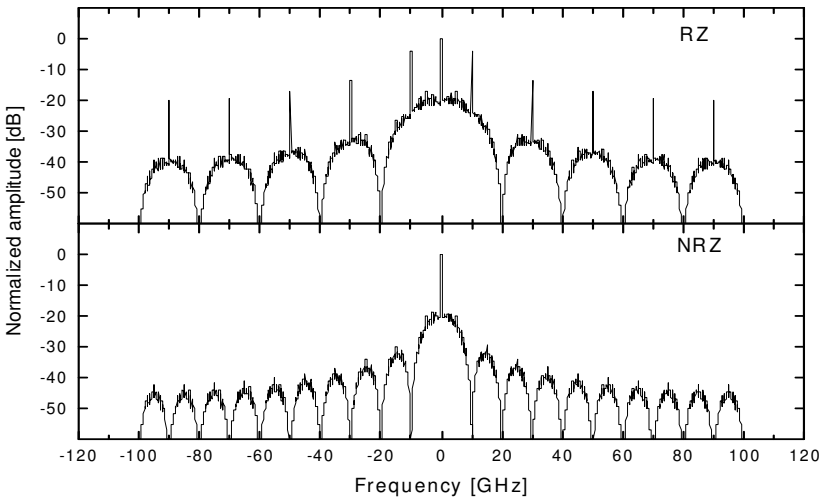

Figure 5-2 **Comparison of the channel spectra relative to the carrier frequency of two PRBS with one channel using return-to-zero modulation and the other non-return-to-zero modulation scheme. One should notice the presence of the strong spectral components of the RZ-modulation at the bit-rate and its odd harmonics.**

Publication P7 presents a possible realization of a resonator-based multi-channel CR. In the work, a F-P resonator is tuned in such a manner that the sideband of the RZ modulation sideband of a WDM channels coincides with one of the resonator fringes. Subsequently, the signal is coupled together with an unmodulated original channel carrier frequency. This can be coupled, filtered and amplified from the transmitted optical signal or completely generated at the receiver end of the system. Once these two signals are coupled together, the beat signal will emerge. In the demonstration in P7, the unmodulated carrier signals were simply branched from the transmitter before the external modulators. This method would naturally be unrealistic in true long haul transmission systems.

The feasibility of creating an accurate enough copy of the carrier frequency at the receiver can be questionable without novel innovations. However, the system is directly scalable to recover the clock signals from multiple wavelength channels with a single F-P resonator, which makes the system interesting despite the unsolved shortcoming. One promising innovation to resolve the issue is the implementation of a birefringent resonator [P6].

6.2 Advantages of birefringent resonators in clock recovery

In the work presented in P6, a solution is offered to both the trilemma of tuning the resonator effective length to satisfy the requirements of multichannel CR and to the realization of the unmodulated carrier frequencies at the receiver. The proposed modification to the setup described in P7 is the use of a birefringent F-P resonator. The resonator used in the experiment was a piece of single mode fiber with dielectric mirrors deposited on the end facets of the fiber. Mechanical pressure was applied to

the side of the fiber leading to the creation of a slow axis in the direction of the force and fast axis perpendicular to the slow axis. A fiber with deliberately built-in birefringence, realized with stress-applying regions or an elliptical core, would have been an alternative option. Incident light is launched to the resonator preferably at an angle of 45° relative to the two axes as illustrated in Fig. 5-3. At the output of the resonator, a polarizer can be utilized to make sure light from both axes is collected.

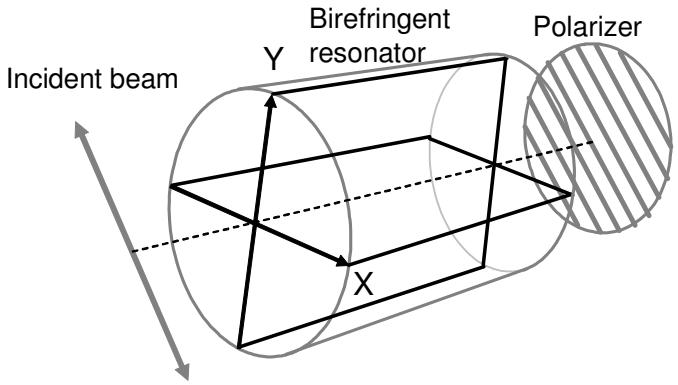

Figure 5-3 **Incident light is launched in to the resonator at an angle so that both polarization modes, X and Y, are excited. At the output of the resonator, light from both polarization modes are selected to achieve a clock beat signal.**

To tune the birefringent resonator for multichannel CR, the birefringence, as in the separation of the two polarization modes, is modified to match the bit-rate of the channels. The resonator length on the other hand is chosen so that the FSR, or its integer multiple, matches the channel spacing. A simulation of a channel signal before and after being processed by the birefringent resonator is presented in Fig. 5-4. Only two dominant spectral features remain after the signal has passed the resonator. These spectral lines will create a low frequency beat signal at precisely the clock frequency.

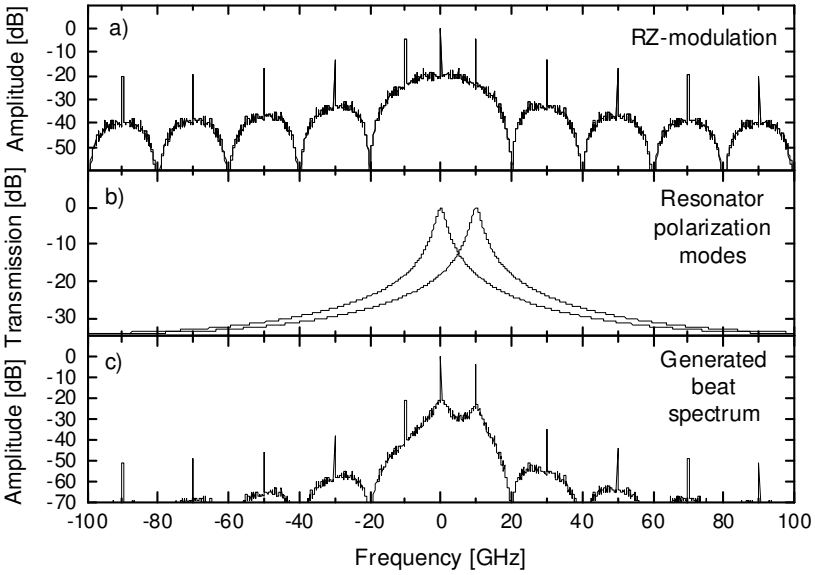

Figure 5-4 **The simulated spectrum of RZ PRBS modulation (a) is launched in to a birefringent resonator where the incident light is divided between the two polarization modes of the F-P resonator (b). At the output, majority of the spectral components are attenuated for except two spectral components (c) that form a beat signal at the clock frequency.**

The feasibility of the proposed CR scheme was demonstrated by simultaneously recovering the clock signal from a multiplex of 20 WDM channels operating at 10 Gb/s each [P6].

7 Summary

This thesis explored novel optical methods and devices designed for the wavelength division multiplexed optical transmission systems of tomorrow. The presented devices were based on Fabry-Perot resonators and photonic crystal fibers. The common goal of the various device concepts was to achieve good performance with new, simple and cost-effective solutions.

A solid silicon based wavelength reference for the fiber-optic telecommunication wavelength region was designed and its performance was characterized. The silicon resonators were fabricated by VTT and comprised of dielectric mirrors and thin film resistors deposited on the surface of a double side polished silicon wafer chip. The concentric heating and sensing resistors together with the high-resolution temperature tuning circuitry provided means to rapidly tune and stabilize the transmission of the artifact with femtometer-scale resolution. The device was calibrated using molecular absorption lines of acetylene resulting in an achievable absolute accuracy of around 1 pm across the whole wavelength range used for long-haul optical telecommunications. Later, we took the device further in publication [P2] by combining it with a patented sampling scheme [55] to monitor both the wavelengths and power levels of DWDM transmission channels directly from the optical multiplex [56].

We successfully demonstrated the gas-filling of PBFs and proved their potential to function as gas sensors [P4] or wavelength reference artifacts [P3]. We were the first to explore the available gases for referencing the ITU-T recommended DWDM channel wavelengths using gas-filled PBFs and presented measurement results of realized reference fibers [78]. The performance of the references was compared with the performance of traditional absorption cells of equal length and pressure. The motivation for such reference fibers came from the possibility to use a long interaction length for added sensitivity combined with a low gas pressure for improved resolution. Also, the devices are naturally readily all-fiber devices and are therefore easily integrated to other existing fiber optic systems.

A realized all-optical switch based on a LC-filled PBF was presented in publication [P5]. The device made use of a transverse aligning geometry that enables the use of 1.55 μm region signals to optically control 1.55 μm region channels with no measurable crosstalk.

We presented new means to extract the clock signals all-optically with a single passive device directly from the DWDM multiplex signal [P6, P7]. The method was based on a high finesse fiber resonator made from standard single-mode fiber and with the pressure-induced birefringence tuned to the modulation frequency of the channel bit-rate. This generated a beat signal that was equal in frequency with the original data clock.

References

1. J. H. Hett and L. E. Curtiss, "Fiber optics duodenoscope and ureterscope", J. Opt. Soc. Am. **51**, 581-582 (1961).

2. N. Nobukazu, "Recent progress in glass fibers for optical communication", Jpn. J. Appl. Phys **20**, 1347-1360 (1981).

3. ITU-T standard G.694.1, *Spectral grids for WDM applications: DWDM frequency grid.*

4. W. H. Wollaston, "A method of examining refractive and dispersive powers by prismatic reflection", Phil. Trans. R. Soc. **92**, 365-380 (1802).

5. C. Fabry and A. Pérot, "Sur les franges des lames minces argentées et leur application à la mesure de petites épaisseurs d'air", Ann. Chim. Phys. **12**, 459-501 (1897).

6. J. C. Knight, T. A. Birks, P. St. J. Russell, and D. M. Atkin, "All-silica single-mode optical fiber with photonic crystal cladding", Opt. Lett. **21**, 1547-1549 (1996).

7. K. J. Blow, N. J. Doran, B. K. Nayar, and B. P. Nelson, "Two-wavelength operation of the nonlinear fiber loop mirror", Opt. Lett. **15**, 248-250 (1990).

8. M. C. Farries and D. N. Payne, "Optical fiber switch employing a Sagnac interferometer", Appl. Phys. Lett. **55**, 25-26 (1989).

9. P. A. Champert, S. V. Popov, and J. R. Taylor, "Generation of multiwatt, broadband continua in holey fibers", Opt. Lett. **27**, 122-124 (2002).

10. S. Coen, A. H. Lun Chau, R. Leonhardt, J. D. Harvey, J. C. Knight, W. J. Wadsworth, and P. St. J. Russell, "White-light supercontinuum generation with 60-ps pump pulses in a photonic crystala fiber", Opt. Lett. **26**, 1356-1358 (2001).

11. J. M. Dudley, G. Genty, and S. Coen, "Supercontinuum generation in photonic crystal fiber ", Reviews of Modern Physics **78**, 1135-1185 (2006).

12. G. Genty, M. Lehtonen, H. Ludvigsen, J. Broeng, and M. Kaivola, "Spectral broadening of femtosecond pulses into continuu, radiation in microstructured fibers", Opt. Express **10**, 1083-1098 (2002).

13. R. F. Cregan, B. J. Mangan, J. C. Knight, T. A. Birks, P. St. J. Russell, P. J. Roberts, and D. C. Allan, "Single-mode photonic band gap guidance of light in air", Science **285**, 1537-1539 (1999).

14. T. T. Alkeskjold, J. Laegsgaard, A. Bjarklev, D. S. Hermann, A. Anawati, J. Broeng, J. Li, and S-T. Wu, "All optical modulation in dye-doped nematic liquid crystal photonic bandgap fibers", Opt. Express **12**, 5857-5871 (2004).

15. P. Domachuk, H. C. Nguyen, and B. J. Eggleton, "Transverse probed microfluidic switchable photonic crystal fiber devices", IEEE Photonics Technol Lett. **16**, 1900-1902 (2004).

16. F. Du, Y-Q. Lu, and S-T. Wu, "Electrically tunable liquid-crystal photonic crystal fiber", Appl. Phys. Lett. **85**, 2181-2183 (2004).

17. T. T. Larsen, "Optical devices based on liquid crystal photonic bandgap fibres", Opt. Express **11**, 2589 (2003).

18. R. Salem and T.E. Murphy, "Broadband optical clock recovery system using two-photon absoprtion", Photon. Technol. Lett. **16**, 2141-2143 (2004).

19. L. Stampoulidis, E. Kehayas, H. Avramopoulos, Y. Liu, E. Tangdiongga, and H.J.S. Dorren, "40 Gb/s fast-locking all-optical packet clock recovery," in Proceedings of *Optical Fiber Communication Conference, OFC 2005*, in Anaheim, USA, paper OThE2 (2005).

20. D. Colladon and J. Babinet, "On the reflections of a ray of light inside a parabolic liquid stream", Comptes Rendes **15**, 800-802 (1842).

21. W. Wheeler, U.S. Patent: US247229, (1881)

22. K. C. Kao and G. A. Hockham, "Dielectric-fiber surface waveguides for optical frequencies", Proc. Inst. Elect. Eng. **113**, 1151-1158 (1966).

23. F. P. Kapron, D. B. Keck, and R. D. Maurer, "Radiation losses in glass-optical waveguides", Appl. Phys. Lett. **17**, 423-425 (1970).

24. D. B. Keck and A. R. Tynes, "Spectral response of low-loss optical waveguides", Appl. Opt **11**, 1502-1506 (1972).

25. M. Saad and J. S. Tassé, "Fluoride glasses draw fiber into the mid-infrared", Laser Focus World **43**, 105-110 (2007).

26. P. St. J. Russell, "Photonic crystal fibers", Science **299**, 358 (2003).

27. P. St. J. Russell, "Photonic crystal fibers", J. Lightwave Technol. **24**, 4729-4749 (2006).

28. P. V. Kaiser, E. A. J. Marcatili, and S. E. Miller, "A new optical fiber", Bell Syst. Tech. J. **52**, 265-269 (1973).

29. J. C. Knight, J. Broeng, and T. A. Birks, "Photonic band gap guidance in optical fibers", Science **282**, 1476-1478 (1998).

30. B. Alfeeli, G. Pickrell, and A. Wang, "Sub-nanoliter spectroscopy gas sensors", Sensors **6**, 1308-1320 (2006).

31. D. G. Ouzounov, F. R. Ahmad, D. Müller, N. Venkataraman, M. T. Gallagher, M. G. Thomas, J. Silcox, K. W. Koch, and A. L. Gaeta,

"Generation of megawatt optical solitons in hollow-core photonic band-gap fibers ", Science **301**, 1702-1704 (2003).

32. O. E. Delange, "Wideband optical communication systems", Proc. IEEE **58**, 1683-1696 (1970).

33. S. Hata, "An optical filter for fiber transmission systems", Opt. Quantum Electron **9**, 265-267 (1977).

34. K. Nosu and H. Ishio, "A design of optical multi/demultiplexers for optical wavelength-division multiplexing transmission", Trans. IECE **62-B**, 1030-1036 (1979).

35. W. Tomlinson, "Wavelength multiplexing in multimode optical fibers", Appl. Opt **18**, 2180-2194 (1977).

36. ITU-T standard G.694.2, *Spectral grids for WDM applications: CWDM wavelength grid.*

37. C. X. Yu, S. Chandrasek, T. Zhou, and D. T. Neilson, "0.8 bit/s/Hz spectral efficiency at 10 Gbit/s via vestigial-sideband filtering", Electron. Lett. **39**, 225-227 (2003).

38. R. J. Mears, L. Reekie, I. M. Jauncey, and D. N. Payne, "Low-noise Erbium-doped fibre amplifier at 1.54pm", Electron. Lett. **23**, 126-1028 (1987).

39. E. Desurvire, J. Simpson, and P. C. Becker, "High-gain erbium-doped traveling-wave fiber amplifier", Optics Lett. **12**, 888-890 (1987).

40. R. I. Laming, M. C. Farries, P. R. Morkel, L. Reekie, and D. N. Payne, "Efficient pump wavelengths of erbium-doped optical fiber amplifier", Electron. Lett. **25**, 12-14 (1989).

41. B. Pedersen, M. L. Dakss, B. A. Thompson, W. J. Miniscalco, T. Wei, and KL. J. Andrews, "Experimental and theoretical analysis of efficient erbium-doped fiber power-amplifiers", Photon. Technol. Lett. **3**, 1085-1087 (1991).

42. E. Desurvire, J. L. Zyskind, and C. R. Giles, "Design optimization for efficient erbium-doped fiber amplifiers", J. Lightwave Technol. **8**, 1730-1741 (1990).

43. T. Miyazaki, Y. Karasawa, and M. Yoshida, "Neodymium-doped fibre amplifier at 1.064 μm", Electron. Lett. **30**, 2142-2143 (1994).

44. R. Paschotta, J. Nilsson, A. C. Tropper, and D. C. Hanna, "Ytterbium-doped fibre amplifiers", IEEE J. Quant. Electr. **33**, 1049-1056 (1997).

45. C. Berkdemir and S. Özsoy, "Modelling consideration of praseodymium-doped fiber amplifiers for 1.3 μm wavelength applications", Opt. Commun. **269**, 120-106 (2006).

46. T. Kasamatsu, Y. Yano, and T. Ono, "1.49-μm-band gain-shifted thulium-doped fiber amplifier for WDM transmission systems ", J. Lightwave Technol. **20**, 1826-1838 (2002).

47. A. L. Cauchy, "Sur la refraction et la réflexion de la lumière", Bull. Sci. Math. **14**, 6-10 (1830).

48. W. Sellmeier, "Theorie der anomal licht-dispersion", Ann. Phys. Chem. **143**, 271-282 (1871).

49. T. Niemi, S. Tammela, T. Kajava, M. Kaivola, and H. Ludvigsen, "Temperature-tunable silicon-wafer etalon for frequency chirp measurements", Microwave and Optical Technol. Lett. **20**, 190-192 (1999).

50. T. Niemi, M. Uusimaa, S. Tammela, P. Heimala, T. Kajava, M. Kaivola, and H. Ludvigsen, "Tunable silicon etalon for simultaneous spectral filtering and wavelength monitoring of a DWDM transmitter", IEEE Photonics Technol Lett. **13**, 58-60 (2001).

51. G. Hawkins, *Spectral characterisation of infrared optical materials and filters*. 1998, University of Reading.

52. E. Palik, *Handbook of optical constants of solids*. 1985: Academic Press.

53. T. Niemi, S. Tammela, and H. Ludvigsen, "Device for frequency chirp measurements of optical transmitters in real time", Rev. Sci. Instrum. **73**, 1103-1107 (2002).

54. J. Tuominen, T. Niemi, P. Heimala, and H. Ludvigsen, "Compact wavelength reference for optical telecomunication based on a tunable silicon etalon," in Proceedings of *International Union of Radio Science - XXVIIth General Assembly (URSI'02)*, in Maastricht, The Netherlands, paper p1512 (2002).

55. A. Pietiläinen, M. Söderlund, and S. Tammela, (WO/2002/051090), (2002)

56. M. Söderlund, J. Tuominen, T. Niemi, H. Ludvigsen, and M. Leppihalme, "Device concept for monitoring DWDM channels," in Proceedings of *the 29th European Conference on Optical Communication and 14th International Conference on Integrated Optics and Optical Fibre Communication (ECOC-IOOC '03)*, in Rimini, Italy, paper We3.2.2 (2003).

57. J. R. de Laeter, J. K. Böhlke, P. De Bièvre, H. Hidaka, H. S. Peiser, K. J. R. Rosman, and P. D. P. Taylor, "Atomic weights of the elements. Review 2000 (IUPAC Technical Report)", Pure Appl. Chem. **75**, 683-799 (2003).

58. R. El Hachtouki and J. Vander Auwera, "Absolute line intensities in acetylene: The 1.5-um region", J. Mol. Spectrosc. **216**, 355-362 (2002).

59. L. Fusina, F. Tamassia, and G. di Lonardo, "The infrared spectrum of 12C2HD: the stretching-bending combination bands in the 1800-4700 cm^{-1} region", Molec. Phys. **103**, 2613-2620 (2005).

60. M. Herman, C. Depiesse, G. di Lonardo, A. Fayt, L. Fusina, D. Hurtmans, S. Kassi, M. Mollabashi, and J. Vander Auwera, "The vibration-rotation spectrum of 12C2HD: new overtone bands and global vibrational analysis", J. Molec. Spectrosc. **228**, 499-510 (2004).

61. M. Herman, M. I. El Idrissi, A. Pisarchik, A. Campargue, A.-C. Gaillot, L. Biennier, G. di Lonardo, and L. Fusina, "The vibrational energy levels in acetylene. III 12C2D2", J. Chem. Phys. **108**, 1377-1389 (1998).

62. J. Liévin, M. Abbouti Temsamani, P. Gaspard, and M. Herman, "Overtone spectroscopy and dynamics in monodeuteroacetylene (C_2HD)", Chem. Phys. **190**, 419-445 (1994).

63. W. C. Swann and S. L. Gilbert, "Pressure-induces shift and broadening of 1510-1540 nm acetylene wavelength calibration lines", J. Opt. Soc. Am B **17**, 1263-1270 (2000).

64. M. Kusaba and J. Henningsen, "The ν1+ν3 and the ν1+ν2+ν4(1)+ν5(−1) combination bands of 13C2H2. Linestrengths, broadening parameters, and pressure shifts", J. Mol. Spectrosc. **209**, 216-227 (1999).

65. P. J. Roberts, F. Couny, H. Sabert, B. J. Mangan, D. P. Williams, L. Farr, M. W. Mason, A. Tomlinson, T. A. Birks, J. C. Knight, and P. S-J Russell, "Ultimate low loss of hollow-core photonic crystal fibres", Opt. Express **13**, 236-244 (2005).

66. G. Humbert, J. C. Knight, G. Bouwmans, P. S-J. Russell, D. P. Williams, P. J. Roberts, and B. J. Mangan, "Hollow core photonic crystal fibers for beam delivery", Opt. Express **12**, 1477-1484 (2004).

67. O. Lehmann, "Über fliessende Krystalle", Zeitschrift für Physikalische Chemie **4**, 462-472 (1889).

68. F. Reinitzer, "Beiträge zur Kenntniss des Cholesterins", Monatshefte für Chemie (Wien) **9**, 421-441 (1888).

69. J. L. Fergason, Nematic liquid crystal twist cell display, (1971)

70. H. Kelker and B. Scheurle, "A liquid-crystalline (nematic) phase with a particularly low solidification point", Angewandte Chemie, International Edition **8**, 884-884 (1969).

71. T. Ritari, G. Genty, and H. Ludvigsen, "Supercontinuum and gas cell in a single microstructures fiber", Opt. Lett. **30**, 3380-3382 (2005).

72. M. Lelek, F. Louradour, V. Couderc, P. Viale, S. Février, J. L. Auguste, J. M. Blondy, and A. Barthélémy, "High sensitivity autocorreletor based on a flourescent liquid core fiber", Appl. Phys. Lett. **89**, 061117 (2006).

73. B. J. Eggleton, C. Kerbage, P. S. Westbrook, R. Windeler, and A. Hale, "Microstructured optical fiber devices", Opt. Express **9**, 698-713 (2001).

74. J. Laegsgaard, "Gap formation and guided modes in photonic bandgap fibers with high-index rods", J. Opt. A: Pure Appl. Opt. **6**, 798-804 (2004).

75. H. Nguyen, P. Domachuk, B. Eggleton, M. Steel, M. Straub, M. Gu, and M. Sumetsky, "A new slant on photonic crystal fibers", Opt. Express **12**, 1528-1539 (2004).

76. H. C. Nguyen, P. Domachuk, M. J. Steel, and B. J. Eggleton, "Experimental and finite-difference time-domain technique characterization of transverse in-line photonic crystal fiber", Photon. Technol. Lett. **16**, 1852-1854 (2004).

77. H. Hoffrén, J. Tuominen, and H. Ludvigsen, "All-optical switching in liquid-crystal filled lead silicate photonic crystal fiber using transverse coupling geometry," in Proceedings of *33rd European Conference on Optical Communication (ECOC 2007)*, in Berlin, Germany, paper We.6.1.6 (2007).

78. T. Ritari, J. Tuominen, J. C. Petersen, T. P. Hansen, and H. Ludvigsen, "Miniature wavelength references based on gas-filled photonic bandgap fibers," in Proceedings of *30th European Conference on Optical Communications (ECOC '04)*, in Stockholm, Sweden, paper Mo3.3.2 (2004).

Abstracts of publications

[P1] J. Tuominen, T. Niemi, and H. Ludvigsen, "Wavelength reference for optical communications based on a temperature-tunable silicon etalon", Rev. Sci. Instrum. **74**, 3620-3623 (2003).

We report on a tunable wavelength reference artifact for optical telecommunications based on a solid silicon Fabry-Perot etalon. The principle of operation is presented and the performance is evaluated. The accuracy of the device is measured using comparison against primary references.

[P2] J. Tuominen, M. Söderlund, T. Niemi, M. Leppihalme, and H. Ludvigsen, "Device for simultaneous monitoring of the channel wavelengths and power levels in a DWDM system", J. Opt. Netw. **3**, 501-509 (2004).

We report on a device concept for monitoring the wavelengths and power levels of WDM channels making use of a scanning high precision silicon etalon and a digital filter utilizing pilot tones to identify the WDM channels. The proposed system is highly cost-effective utilizing a minimum of components.

[P3] J. Tuominen, T. Ritari, J. Petersen, and H. Ludvigsen, "Gas filled photonic bandgap fibers as wavelength references", Opt. Commun. **255**, 272-277 (2005).

We demonstrate that air-guiding photonic bandgap fibers filled with gases like acetylene and methane provide compact wavelength references. The long natural interaction length provides means to explore unconventional absorption bands to find suitable lines for referencing DWDM channels.

[P4] T. Ritari, J. Tuominen, J.C. Petersen, T. Sørensen, T.P. Hansen, H. Simonsen, and H. Ludvigsen, "Gas sensing using air-guiding photonic bandgap fibers", Opt. Express **12**, 4080-4087 (2004).

We report on successful experiments of filling the air holes of photonic bandgap fibers with selected trace-gases, sealing the filled fibers and measuring the transmission spectra. The feasibility of optical fibers for the use of spectroscopy is evaluated.

[P5] J. Tuominen, H. Hoffrén, and H. Ludvigsen, "All-optical switch based on liquid-crystal infiltrated photonic bandgap fiber in transverse configuration", JEOS:RP **2**, 07016 (2007).

We report on an optical switch based on transversally transmitting photonic bandgap fibers filled with liquid crystal. The extinction ratios of the switch are measured for various geometries. The realized all-optical switch is shown to have an exceptionally wide operating band.

[P6] T. von Lerber, J. Tuominen, H. Ludvigsen, S. Honkanen, and F. Küppers, "Multichannel and rate all-optical clock recovery", IEEE Photonics Technol. Lett. **18**, 1395-1397 (2006).

We report on the utilization of a birefringent Fabry-Perot resonator to extract the clock signals of 20 WDM channels simultaneously . Multi-rate clock recovery is also demonstrated for 10 and 40 Gb/s systems.

[P7] T. von Lerber, J. Tuominen, H. Ludvigsen, S. Honkanen, and F. Kueppers, "Investigation of multiwavelength clock recovery based on heterodyne beats of sideband-filtered signal", Opt. Commun. **271**, 87-90 (2007).

We report on multichannel all-optical clock recovery using a single Fabry-Perot fiber-resonator to perform the clock recovery operation simultaneously for all channels in a 20-channel WDM system.

ISBN 978-951-22-9650-7
ISBN 978-951-22-9651-4 (PDF)
ISSN 1795-2239
ISSN 1795-4584 (PDF)